Final Report

CRITICAL ISSUES RELATED TO CORROSION INDUCED DETERIORATION PROJECTION FOR CONCRETE MARINE BRIDGE SUBSTRUCTURES

submitted to

Florida Department of Transportation Research Center
605 Suwannee Street
Tallahassee, Florida 32399

submitted by

William H. Hartt, Jingak Nam, and Lianfang Li
Center for Marine Materials
Department of Ocean Engineering
Florida Atlantic University – Sea Tech Campus
101 North Beach Road
Dania Beach, Florida 33004

December 30, 2002

EXECUTIVE SUMMARY

A series of 91 concrete G109 type specimens were exposed to cyclic wet-dry ponding with either a 15 w/o NaCl solution or natural sea water for as long as four years. Mix design variables included 1) cement alkalinity (equivalent alkalinities of 0.97 (high), 0.52 (normal and typical of cements used for Florida bridges), and 0.36 (low)), 2) water cement ratio (0.50, 0.41, and 0.37), 3) presence versus absence of coarse aggregate, and 4) presence versus absence of fly ash. Corrosion potential and macrocell current between bottom and top bars were periodically monitored in order to determine the time at which active corrosion commenced. Subsequent to corrosion initiation, specimens were autopsied and determinations made of 1) the effective chloride diffusion coefficient, 2) pore water pH, and 3) the critical chloride concentration for corrosion initiation was calculated.

The time for corrosion to initiate conformed to a distribution that was represented by Weibull statistics. The mean time-to-corrosion for specimens fabricated using the high alkalinity cement was approximately ten times greater than for those fabricated from the normal and low alkalinity ones. Consequently, since alkali silica reaction is generally not a problem in the State, specification of high alkalinity cements for bridge construction should lead to significantly enhanced resistance to corrosion induced concrete deterioration at no additional cost.

In cases where determinations were made, corrosion initiated at a macro-void that happened to be present on the top side of the reinforcing steel. This is thought to have occurred in conjunction with a corrosion cell established between the contiguous concrete covered and void area steel, where the former served as a cathode and the latter as an anode. On this basis, time-to-corrosion was influenced by the size and density of such voids. The possibility is explored that additional corrosion resistance could be realized by void control, as might be affected by modified placement procedures and inclusion of admixtures designed to reduce void size and density.

TABLE OF CONTENTS

LIST OF TABLES

LIST OF FIGURES

Page

INTRODUCTION

Overview of Concrete Deterioration Processes

General

While concrete has evolved to become the most widely used structural material in the world, the fact that its capacity for plastic deformation is essentially nil imposes major practical design limitations. This shortcoming is most commonly overcome by incorporation of steel reinforcement into those locations in the concrete where tensile stresses are anticipated. Consequently, concerns regarding performance must not only focus upon properties of the concrete per se but also of the embedded steel and, in addition, the manner in which these two components interact. In this regard, steel and concrete are in most aspects mutually compatible, as exemplified by the fact that the coefficient of thermal expansion for each is approximately the same. Also, while boldly exposed steel corrodes actively in most natural environments at a rate that requires use of extrinsic corrosion control measures (for example, protective coatings for atmospheric exposures and cathodic protection in submerged and buried situations), the relatively high pH of concrete pore water (pH ≈ 13.0-13.8) promotes formation of a protective passive film such that corrosion rate is negligible and decades of relatively low maintenance result.

Corrosion Mechanism

Disruption of the passive film upon embedded reinforcement and onset of active corrosion can arise in conjunction with either of two causes: carbonation or chloride intrusion (or a combination of these two factors). In the former case (carbonation), atmospheric carbon dioxide (CO_2) reacts with pore water alkali according to the generalized reaction,

$$Ca(OH)_2 + CO_2 \rightarrow CaCO_3 + H_2O, \qquad (1$$

which consumes reserve alkalinity and eventually reduces pore water pH to the 8-9 range, where steel is no longer passive. For dense, high quality concrete (for

example, high cement factor, low water-cement ratio, and presence of a pozzolanic admixture) carbonation rates are typically on the order of one mm per decade or less; and so loss of passivity from this cause within a normal design life is not generally a concern. On the other hand, carbonation is often a problem for older structures; first, because of age per se and, second, because earlier generation concretes were typically of relatively poor quality (greater permeability) than more modern ones.

Chlorides, on the other hand, arise in conjunction with deicing activities upon northern roadways or from coastal exposure (or both). While this species (Cl^-) has only a small influence on pore water pH per se, concentrations as low as 0.6 kg/m^3 (1.0 pcy) (concrete weight basis) have been projected to compromise steel passivity (1,2). In actuality, it is probably not the concentration of chlorides per se that governs loss of passivity but rather some function of the chloride-to-hydroxide ratio ($[Cl^-]/[OH^-]$), since the latter species (OH^-) is prevalent in pore water and acts as an inhibitor. This has been demonstrated by aqueous solution experiments from which it is apparent that the Cl^- threshold for loss of steel passivity increases with increasing pH (3-8). On this basis, the relative amount of cement in a concrete mix and cement alkalinity are likely to affect the onset of corrosion. Considerable research effort has been focused upon identification of a chloride threshold; however, a unique value for this parameter has remained illusive, presumably because of the role of cement, concrete mix, environmental, electrochemical potential, and reinforcement (composition and microstructure) variables that are influential (9,10). Because Cl^- and not carbonation induced loss of passivity is of primary concern for modern bridge structures, subsequent focus in this report is upon this corrosion cause.

Once steel in concrete becomes active, either in conjunction with chlorides achieving a threshold concentration or pore solution pH reduction from carbonation at the embedded steel depth, then the classical anodic iron reaction,

$$Fe \rightarrow Fe^{+2} + 2e^- , \qquad (2$$

and cathodic oxygen reaction,

$$\frac{1}{2}O_2 + H_2O + 2e^- \rightarrow 2OH^-, \quad (3$$

occur at an accelerated rate. Despite the normally high alkalinity of concrete, acidification may occur in the vicinity of anodic sites because of oxygen depletion and hydrolysis of ferrous ions. Thus,

$$Fe^{+2} + 2H_2O \rightarrow Fe(OH)_2 + 2H^+. \quad (4$$

The product H^+ may be reduced and, along with O_2 reduction at more remote cathodic sites, further stimulate the anodic process. Irrespective of this, the net reaction is

$$Fe + \frac{1}{2}O_2 + H_2O \rightarrow Fe^{+2} + 2OH^- \rightarrow Fe(OH)_2 \quad (5$$

and, upon further oxidation,

$$2Fe(OH)_2 + \frac{1}{2}O_2 + H_2O \rightarrow 2Fe(OH)_3, \quad (6$$

in addition to,

$$2Fe(OH)_3 \rightarrow Fe_2O_3 + 3H_2O, \quad (7$$

as drying takes place.

Corrosion per se is seldom the cause of failure in reinforced concrete components and structures. This arises because the final corrosion products (either ferric oxide or hydroxide) have a specific volume that is several times greater than that of the reactant steel; and accumulation of these in the concrete pore space adjacent to anodic sites leads to development of tensile hoop stresses about the steel which, in combination with the relatively low tensile strength of concrete (typically 1-2 MPa), ultimately causes cracking and spalling.

Damage of this type has evolved to become a significant concern in the case of coastal bridge sub-structures in Florida. Figure 1 illustrates the deterioration process schematically where chlorides accumulate within the submerged zone from inward sea water migration and in the atmospheric zone as a consequence of capillary flow, splash, and spray. The lack of dissolved oxygen in the submerged zone precludes Reaction 2, and so corrosion is rarely a problem here. However, ready availability of both Cl^- in the splash zone and of O_2 at contiguous, more elevated locations results in this location (splash zone) being particularly susceptible to corrosion induced damage. Figure 2 shows a photograph of a marine bridge piling that exemplifies this.

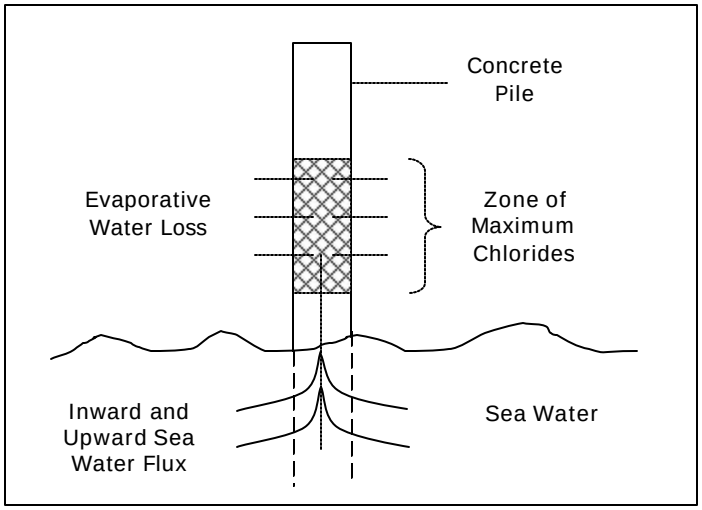

Figure 1: Schematic illustration of sea water migration and Cl^- accumulation within a marine piping.

Representation of Corrosion Induced Concrete Deterioration

Corrosion induced deterioration of reinforced concrete can be modeled in terms of three component steps: 1) time for corrosion initiation, 2) time, subsequent to corrosion initiation, for corrosion propagation (appearance of a crack on the external concrete surface), and 3) time for one or more surface cracks to develop into spalls that require repair, rehabilitation, or replacement. Figure 3 illustrates these schematically as a plot of cumulative damage versus time showing the above three component times, T_i, T_p, and T_d (periods for initiation, propagation, continued damage (spalling), respectively), as well as the time-to-failure, T_f, or functional service life (modified from Tutti (11)). Of the former three terms, T_i typically

Figure 2: Photograph of a cracked and spalled marine bridge piling.

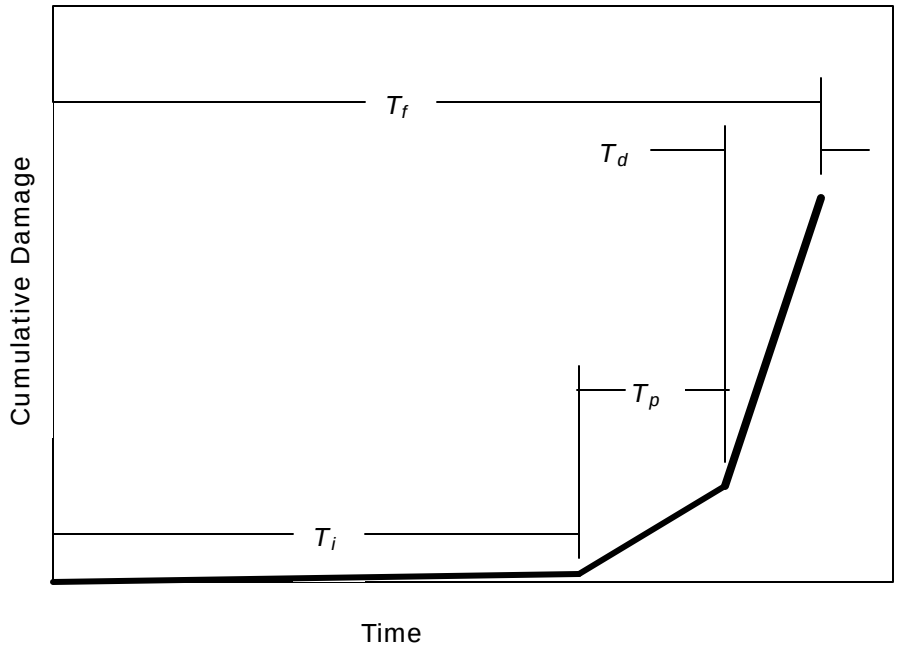

Figure 3: Schematic illustration of the various steps in deterioration of reinforced concrete due to chloride induced corrosion.

occupies the longest period; and so it is upon this parameter that corrosion control measures generally focus. The approach adapted by the Florida Department of

Transportation for new bridge construction is to extend the time-to-corrosion initiation by a combination of 1) adequate concrete cover and 2) use of high performance concretes; that is, concretes with permeability reducing (pozzolanic) or corrosion inhibiting admixtures (or both). Likewise, the methods of Life-Cycle Cost Analysis (LCCA) are employed to evaluate and compare different materials selection and design options. This approach considers both initial cost and the projected life history of maintenance, repair, and rehabilitation expenses that are required until the design life is reached. These are then evaluated in terms of the time value of money, from which Present Worth is determined. Comparisons between different options can then be made on a normalized basis. Figure 4 graphically illustrates an example life-cycle cost scenario.

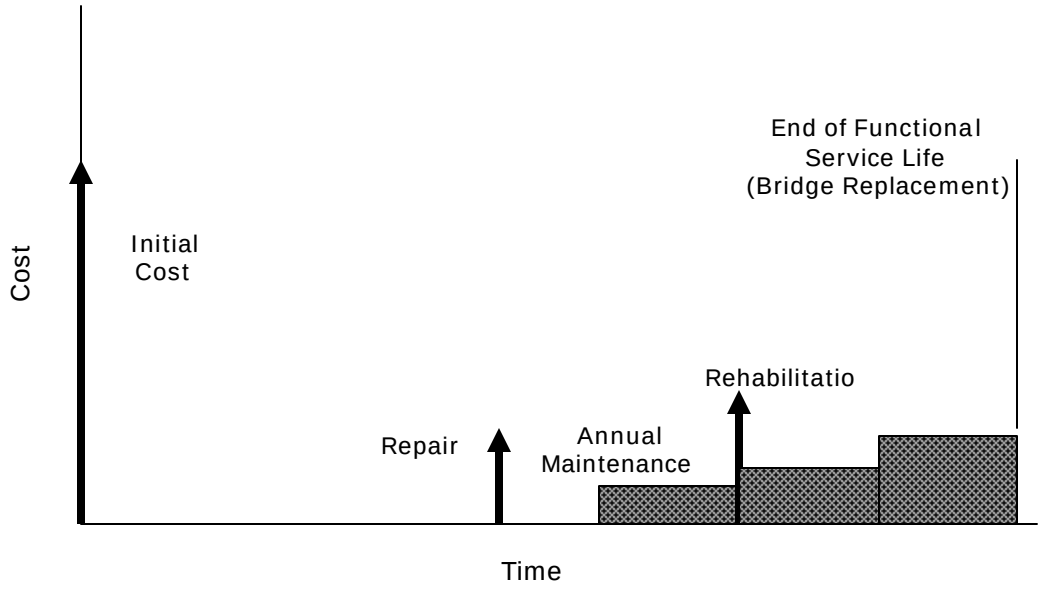

Figure 4: Schematic illustration of life cycle cost.

Analysis of Corrosion Initiation (Time-to-Corrosion)

General

Electrolyte composition is invariably a dominant factor affecting any corrosion process, including that for steel in concrete. As noted above, the predominant corrosion activator in concrete pore water is normally chlorides, whereas hydroxides serve as a passivator. Consequently, T_i for concrete structures is determined by the

competing influences of these two species. On the one hand, pore water pH is affected by cement content, cement alkalinity, and exposures that promote carbonation. On the other, chloride concentration, $[Cl^-]$, at the steel depth is determined by 1) composition of this species in the environment, 2) its ingress rate into concrete, and 3) concrete cover over the steel, with onset of active corrosion defined by the Cl^- threshold concentration for passive film breakdown, c_{th}.

Pore Water pH

Corrosion experiments intended to simulate steel in concrete have historically employed a saturated $Ca(OH)_2$ solution, the pH of which is approximately 12.4. However, with the advent of the pore water expression method (12-14) and theoretical considerations, it was recognized that K^+ and Na^+ are the predominant cations; and the solubility and concentration of these is such that a pH in excess of 13 typically occurs.

Limitations associated with pore water expression include, first, prior water saturation of samples is required and, second, the method is more useful for pastes and mortars since expression yields for concrete, particularly high performance ones, is low. Consequently, both ex-situ and in-situ leaching methods (15,16) have also been developed, where the former involves exposure of a powder sample to distilled water and the latter placement of a small quantity of water into a drilled cavity in hardened concrete. A limitation in the case of ex-situ leaching is that solid $Ca(OH)_2$ from the concrete becomes dissolved and elevates $[OH^-]$ compared to what otherwise would occur. Also, the dissolved $Ca(OH)_2$, if saturated, buffers the leachate at a pH of about 12.4. These limitations are minimized by the in-situ method because only about 0.4 mL of distilled water is employed; however, water saturation of the specimen is required here also. Recently, a modification of the ex-situ method was proposed whereby a correction is made for the $[OH^-]$ resulting from $Ca(OH)_2$ dissolution (7,17); however, solubles in unreacted cement particles may also become dissolved, thereby elevating the calculated pH compared to what actually existed in the pore water. Consequently, this procedure may be more a measure of inherent alkalinity than of pore water pH.

Chlorides

The mechanism of Cl^- intrusion into concrete invariably involves both capillary suction and diffusion; however, for situations where the depth to which the former (capillary suction) occurs is relatively shallow compared to the reinforcement cover, diffusion alone is normally considered. Analysis of the latter (diffusion) is accomplished in terms of Fick's second law or,

$$\frac{\partial c(x,T)}{\partial t} = \frac{\partial}{\partial t}\left(D \cdot \frac{\partial c(x,T)}{\partial x}\right), \qquad (8$$

where $c(x,T)$ is $[Cl^-]$ at depth x beneath the exposed surface after exposure time T and D is the diffusion coefficient. As Equation 8 is written, D is assumed to be independent of concentration. The solution in the one-dimensional case is,

$$\frac{c(x,T) - c_o}{c_s - c_o} = 1 - \mathrm{erf}\left(\frac{x}{2\sqrt{D \cdot T}}\right), \qquad (9$$

where

c_o is the initial or background Cl^- concentration in the concrete,
c_s is the Cl^- concentration on the exposed surface, and
erf is the Gaussian error function.

Assumptions involved in arriving at this solution are, first, c_s and D are constant with time and, second, the diffusion is "Fickian;" that is, there are no Cl^- sources or sinks in the concrete. In actuality, c_s may increase with exposure time, although steady-state values in the range 0.3-0.7 (percent of concrete weight) have been projected to result after about six months (18). Factors that effect c_s have been projected to include type of exposure, mix design (cement content, in particular), and curing conditions (19). Also, the diffusion coefficient that is calculated from Equation 9 is an "effective" value, D_{eff}, since it is weighted over the relevant exposure period due, first, to the fact that c_s may vary and, second, because of progressive cement hydration with time, and, lastly, chemical and physical Cl^- binding such that the concrete acts as a sink for this species and some fraction is no longer able to diffuse.

In the approach represented by Equation 9, $c(x,T)$, c_o, and c_s are measured experimentally (normally by wet chemistry analysis) and D_{eff} is calculated based upon knowledge of reinforcement cover and exposure time. Experimental scatter and error may be minimized by measuring $c(x,T)$ at multiple depths and employing a curve-fitting algorithm to calculate D_{eff}. Also, if D_{eff} is known from one sampling set, then c_{th} can be determined by measuring $c(x,T)$ at the reinforcement depth (c_{rd}) at the time and location of corrosion initiation and solving Equation 9 recognizing that for this situation, $c_{rd} \approx c_{th}$. In any case, the parameters that affect Cl^- intrusion rate are c_s, and D_{eff}, both of which depend upon exposure conditions such as relative humidity and time-of-wetness and material variables such as composition and microstructure.

A factor that is not normally considered in time-to-corrosion evaluations is that c_s, x, c_{th}, and D_{eff} are statistically distributed parameters. Consequently, T_i also conforms to some distribution. This is important because decisions regarding repairs and rehabilitations are often made based upon damage having occurred over some percentage of the structure. Alternatively, loss of a single critical, non-redundant structural element (substructure bridge pier, for example) causes failure.

The approach of employing pozzolanic and corrosion inhibiting admixtures that has been adapted by the FDOT for enhancing concrete durability, as noted above, can be related to and interpreted in terms of Equation 9. In this regard, the most prevalent corrosion inhibitor ($Ca(NO_2)_2$), in effect, increases c_{th}, whereas pozzolans (fly ash, silica fume, and blast furnace slag) reduce D_{eff}. Surface [Cl^-] may also be effected by pozzolans.

It is generally recognized that c_{th} increases with increasing cement alkalinity (10), although no systematic investigation that addresses this has been performed. For some geographical locations, concerns regarding alkali-silica reaction (ASR), whereby aggregates swell from a chemical reaction with alkaline pore water, preclude utilizing high alkalinity cements, since ASR should occur at a greater rate the higher the pore water alkalinity. The native Florida limestones that serve as coarse aggregate for concrete bridge construction in most of the State are not susceptible to ASR, however. Consequently, if it can be demonstrated that c_{th} for high alkalinity cements exceeds that for normal ones, then use of these cements

should yield concrete structures with enhanced resistance to corrosion induced deterioration but with no additional cost or construction complexity.

PROJECT DESCRIPTION AND OBJECTIVES

The objectives of this project were to evaluate the extent to which high alkalinity cement in concrete elevates the chloride concentration threshold for breakdown of the passive film upon steel reinforcement and active corrosion initiation and, based upon this, determine the benefits that might be realized in terms of extending time-to-corrosion by using such cements in Florida coastal bridges. The effort involved fabrication of 91 G109 specimens (20) for which mix design variables included 1) cements of three alkalinities, 2) three water-to-cement ratios, 3) presence versus absence of fly ash, and 4) presence versus absence of coarse aggregate. An additional variable was that some specimens were exposed to 15 w/o NaCl and others to natural sea water.

EXPERIMENTAL PROCEDURE

Materials

As noted above, cements of three alkalinities were employed in fabricating the concrete specimens. Table 1 lists the composition for each of these cements. The normal alkalinity one is typical of what is currently employed in bridge construction in Florida. The equivalent alkalinity (*EqA*) for the three cements was determined from the equation,

$$EqA = w/o Na_2O + 0.658 \cdot w/o \cdot K_2O . \qquad (10$$

This revealed values of 0.355 for the "low" alkalinity cement (LA), 0.519 for the "normal" (NA), and 0.972 for the "high" (HA). Table 2 lists the different mix designs.

Specimens

Seven specimens were fabricated for each mix design based upon selected combinations of cement type, water-cement ratio (w/c), and presence versus absence of fly ash and coarse aggregate, where four of these specimens contained reinforcement according to the

Table 1: Compositional analysis results for each of the three cements.

	VALUE, percent		
COMPOUND	LOW	NORMAL	HIGH
SiO_2	21.93	21.88	20.63
Al_2O_3	5.16	5.64	4.44
Fe_2O_3	3.70	3.87	2.56
CaO	65.02	64.42	63.39
MgO	1.39	0.98	3.85
SO_3	2.38	2.87	3.96
Na_2O	0.099	0.164	0.192
K_2O	0.39	0.54	1.19
TiO_2	0.29	0.31	0.22
P_2O_5	0.209	0.123	0.063
Mn_2O_3	0.049	0.038	0.058
SrO	0.09	0.064	0.041
Cr_2O_3	0.003	0.002	0.003
C3A	7.43	8.39	7.43
C2S	24.2	29.3	16.5
C3S	51.255	44.414	56.461
Equivalent Alkalinity	0.355	0.519	0.972

standard G109 design (20) and three were blanks (no reinforcement). Diameter of the reinforcing steel bars was 12.7 mm (#4), and surface preparation involved wire brushing just prior to placement. Table 3 provides a listing of specimens according to the different test categories and indicates individual specimen numbers. The top bar of each reinforced specimen was electrically connected to the two bottom bars through a 100-Ohm shunt and a switch that allowed the circuit to be opened or closed. Figure 5 shows the specimen configuration schematically.

Exposure and Specimen Analyses

A one week wet-one week dry top surface ponding cycle began on June 3, 1998 using a 15 w/o sodium chloride solution for all specimens except for numbers 85-91 for which natural sea water was employed. At the end of the drying cycle, potential and macro-cell current was measured both from the voltage drop across the shunt and by a zero resistance ammeter with the shunt by-passed. Active corrosion was defined initially as having commenced if, for two consecutive data acquisition periods, the macro-cell current was 10 μA or greater and potential for the top bar was –0.28 V_{SCE} or more negative. Later, this definition was relaxed; and active

Table 2: Mix design for concrete specimens.

	Specimen Designation				
	HA,NA,LA-0.37	HA,NA,LA-0.41	HA,NA,LA-0.50	NAF-0.37	NAF-0.41
Batch Materials	kg/m3 (lb/y3)	kg/m3 (lb/y3)	kg/m3 (lb/y3)	kg/m3 (lb/y3)	kg/m3 (lb/y3)
Cement (Type II)	388.4 (657.4)	388.4 (657.4)	388.4 (657.4)	310.7 (526.6)	310.7 (526.6)
Water	143.5 (243.2)	159.0 (269.5)	193.9 (328.7)	143.5 (243.2)	159.0 (269.5)
Fine Aggregate	742.9 (1259.1)	702.0 (1189.8)	610.1 (1034.0)	742.9 (1259.1)	702.0 (1189.8)
Coarse Aggregate	980.1 (1661.1)	980.1 (1661.1)	980.1 (1661.1)	980.1 (1661.1)	980.1 (1661.1)
Fly Ash (Class F)	0	0	0	77.6 (131.5)*	77.6 (131.5)*
Admixtures	kg/cwt (oz/cwt)	kg/cwt (oz/cwt)	kg/cwt (oz/cwt)	kg/cwt (oz/cwt)	kg/cwt (oz/cwt)
WRDA-64	0.51 (6.00)	0.51 (6.00)	0.51 (6.00)	0.51 (6.00)	0.51 (6.00)
WRDA-19	1.70 (20.00)	1.28 (15.00)	0	1.70 (20.00)	1.28 (15.00)
Batch Target Properties**					
Slump, mm (in)	76 (3)	76 (3)	200 (3)	76 (3)	77 (3)
Unit Weight, kg/m^3 (lb/ft^3)	2,254.1 (141.5)	2,228.6 (139.9)	2,171.3 (136.3)	2,254.1 (141.5)	2,228.6 (139.9)
Water-Cement Ratio	0.37	0.41	0.50	0.37	0.41

* Twenty percent cement replacement.

**Air content for all mixes was 4 percent.

Table 3: Listing of specimens according to mix design.

Specimen No.	Reinforcement	Cement Alk.	w/c
01-04, 85-88*	Yes	High	0.37
05-07, 89-91*	No		
08-11	Yes	High	0.41
12-14	No		
15-18	Yes	High	0.5
19-21	No		
22-25	Yes	Normal	0.37
26-28	No		
29-32	Yes	Normal	0.41
33-35	No		
36-39	Yes	Normal	0.5
40-42	No		
43-46	Yes	Low	0.37
47-49	No		
50-53	Yes	Low	0.41
54-56	No		
57-60	Yes	Low	0.5
61-63	No		
64-67	Yes	HAG**	0.50
68-70	No		
71-74	Yes	NAF***	0.37
75-77	No		
78-81	Yes	NAF***	0.41
82-84	No		

* Ponded with natural sea water. All other specimens ponded with 15% NaCl.

** High alkalinity mortar (no coarse aggregate

*** Normal alkalinity cement with 20% fly ash replacement.

corrosion was defined solely in terms of potential having decreased to or become more negative than -0.28 V_{SCE}. After corrosion initiation, specimens were autopsied and the corrosion state assessed. This involved making a saw-cutting lengthwise to a depth of about 50 mm along both sides opposite the top bar and then splitting open the specimen. At certain intervals, a core was taken from within the ponded area of blank specimens (no reinforcing steel) of the different mixes. The cores were then sliced and the individual slices ground to powder. In addition, powder drillings were acquired along the top side of the upper rebar trace at both the corrosion site and elsewhere where the steel remained passive.

Chloride analyses were performed using the FDOT acid soluble method (21).

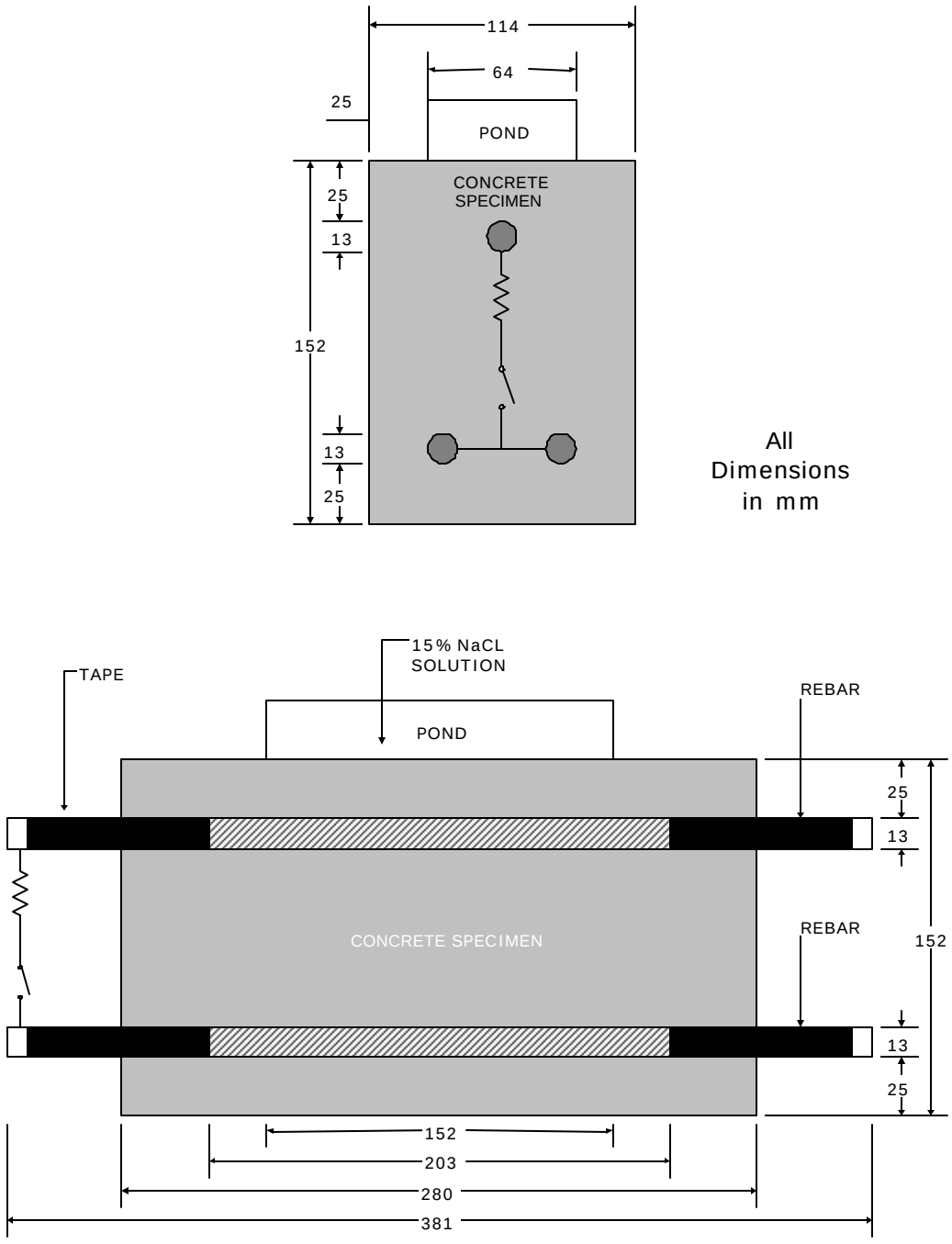

Figure 5: Geometry of the G109 type specimens.

The profile data acquired from the blank specimens were employed in a least-squares curve-fitting algorithm to Equation 9, from which D_{eff} was calculated.

Measurement of pore water pH for samples of each cement alkalinity and w/c

was performed using an ex-situ leaching procedure that was developed in conjunction with FDOT Project WPI 0510716 (7,17). This involved retrieving 5 cm diameter by 15 cm long cores from the Cl^--free portion of representative specimens. The outer one cm thick layer was discarded to avoid concrete that was possibly carbonated, and the core was then pulverized until all material passed a #50 sieve. The concrete powder was divided into approximately 50 g increments with each being stored in an individual air-tight plastic bottle.

For leaching, 50 ml of de-ionized water was added to the individual samples; and then these were mixed and allowed to sit for three days. Separate experiments determined that this leaching time was sufficient for equilibrium to be approached (22). The samples were then filtered to yield about 30 g of liquid. This was divided into two approximately equal parts, each of which was titrated.

The initial titration was for OH^- concentration using 0.1N HCl. This involved measurement of the potential of a combination pH-electrode in the titrated solution and determination of the end-point noted. Immediately after the OH^- titration, pH of the same solution was first adjusted and then titrated for Ca^{2+} concentration using 0.01N EDTA and hydroxy naphthol blue as an indicator. The end point was defined by a change of the solution color from purple to blue. The second solution was titrated identically to the first, and results for the two pairs of titrations were then averaged.

The determination of pore water pH was based upon the following assumptions:

1. The total amount of alkali ions measured in the leachant equals that in the concrete pore water. This assumes that alkali ions have no binding effect similar to that of chlorides.

2. The concrete is fully hydrated.

3. The OH^- in the leachant is balanced by the Na^+ and K^+.

On the basis of the third assumption,

$$[OH^-]_p = [OH^-]_l - 2 \cdot [Ca^{2+}]_l, \quad (11$$

where $[OH^-]_p$ is the concentration of this ion in the leachant that was associated with K^+ and Na^+ in the pore water; and $[OH^-]_l$ and $[Ca^{2+}]_l$ are the respective concentrations in the leachant, as determined from the titrations. Thus, the $[OH^-]$ in concrete pore water ($[OH^-]_{pw}$) can be calculated as,

$$[OH^-]_{pw} = \frac{[OH^-]_l \cdot V_{H_2O}}{\frac{W_{concr}}{d_{concr}} \cdot ?}, \quad (12$$

where

W_{concr} is the total weight of concrete powder used for leaching (g),

V_{H_2O} is the total amount of water used for leaching (ml),

? is concrete porosity (vol. fraction), and

d_{concr} is concrete density, (assumed as 2.3g/cm^3).

The concrete porosity was determined according to ASTM C642-90 (23) for concrete water absorption capacity.

Finally, the concrete pore water pH was calculated from the expression,

$$pH = 14 + \log (?[OH^-]_{pw}), \quad (13$$

where ? is the activity coefficient for OH^-, which is approximately 0.7 when $[OH^-]$ exceeds 0.1 mol/L.

RESULTS AND DISCUSSION

Time-To-Corrosion

At the conclusion of the experiments (July, 2002), 28 of the 52 reinforced G109 specimens had exhibited active corrosion. Table 4 provides a listing of all specimens and of the T_i values in the cases of corrosion activity. In instances where T_i was relatively brief, the shift in corrosion potential, f_{corr}, from the range indicative of passivity (typically f_{corr} more positive than approximately –0.10 V_{SCE}) to that of

Table 4: Specimen times-to-corrosion.

Specimen Number	Mix Design	Time to Corr. (days)		Specimen Number	Mix Design	Time to Corr. (days)
1	HA 0.37	>1,600		43	LA 0.37	>1,600
2	HA 0.37	>1,600		44	LA 0.37	>1,600
3	HA 0.37	>1,600		45	LA 0.37	190
4	HA 0.37	>1,600		46	LA 0.37	>1,600
8	HA 0.41	>1,600		50	LA 0.41	297
9	HA 0.41	1,329		51	LA 0.41	>1,600
10	HA 0.41	1,192		52	LA 0.41	567
11	HA 0.41	1,401		53	LA 0.41	>1,600
15	HA 0.50	136		57	LA 0.50	107
16	HA 0.50	297		58	LA 0.50	234
17	HA 0.50	391		59	LA 0.50	136
18	HA 0.50	225		60	LA 0.50	136
22	NA 0.37	>1,600		64	HAG 0.50	149
23	NA 0.37	>1,600		65	HAG 0.50	178
24	NA 0.37	1,096		66	HAG 0.50	107
25	NA 0.37	1,192		67	HAG 0.50	163
29	NA 0.41	136		71	NAF 0.37	>1,600
30	NA 0.41	206		72	NAF 0.37	>1,600
31	NA 0.41	339		73	NAF 0.37	>1,600
32	NA 0.41	1,120		74	NAF 0.37	>1,600
36	NA 0.50	93		78	NAF 0.41	>1,600
37	NA 0.50	93		79	NAF 0.41	>1,600
38	NA 0.50	136		80	NAF 0.41	>1,600
39	NA 0.50	178		81	NAF 0.41	>1,600

active corrosion (f_{corr} more negative than –0.28 V_{SCE}) (24) was relatively abrupt. Concurrently, macro-cell current increased from negligible to greater than 10 μA. In the case of specimens for which corrosion initiated after a relatively long exposure time, this change was more gradual with specimens often reverting to the passive state. Figure 6 presents potential versus time data for specimens of the LA0.50 mix design, which exemplifies the former type of behavior. Figure 7 presents comparable data for Specimen 24, which typifies the latter. None of the fly ash or sea water ponded specimens have become active. In the former case, this presumably resulted because of reduced D_{eff} and in the latter because of lower [Cl^-] in the sea water compared to 15 w/o NaCl.

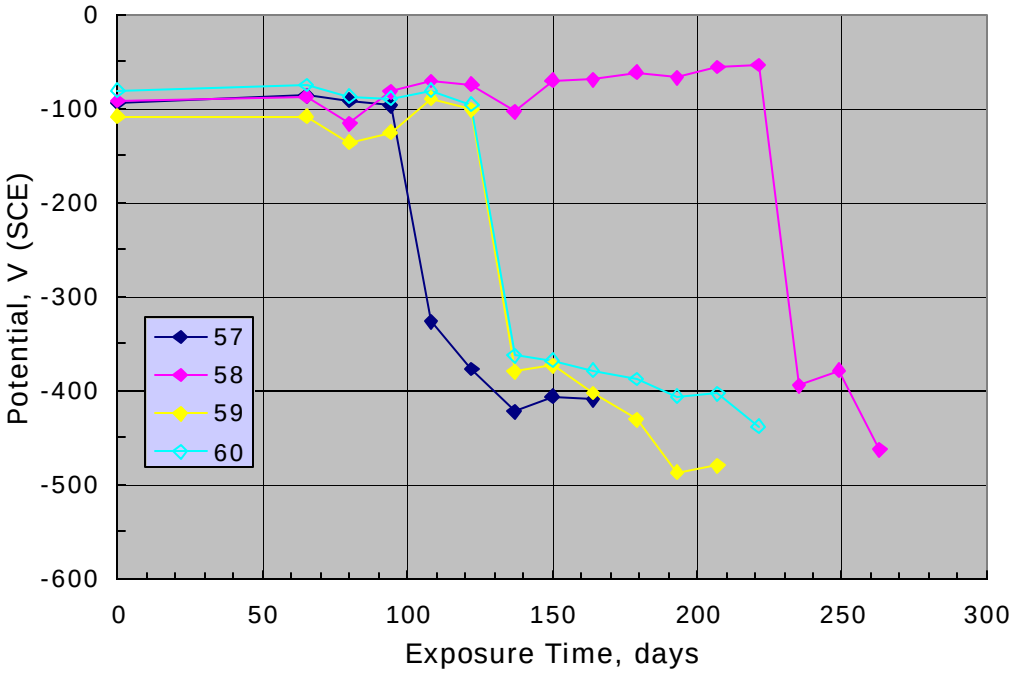

(a)

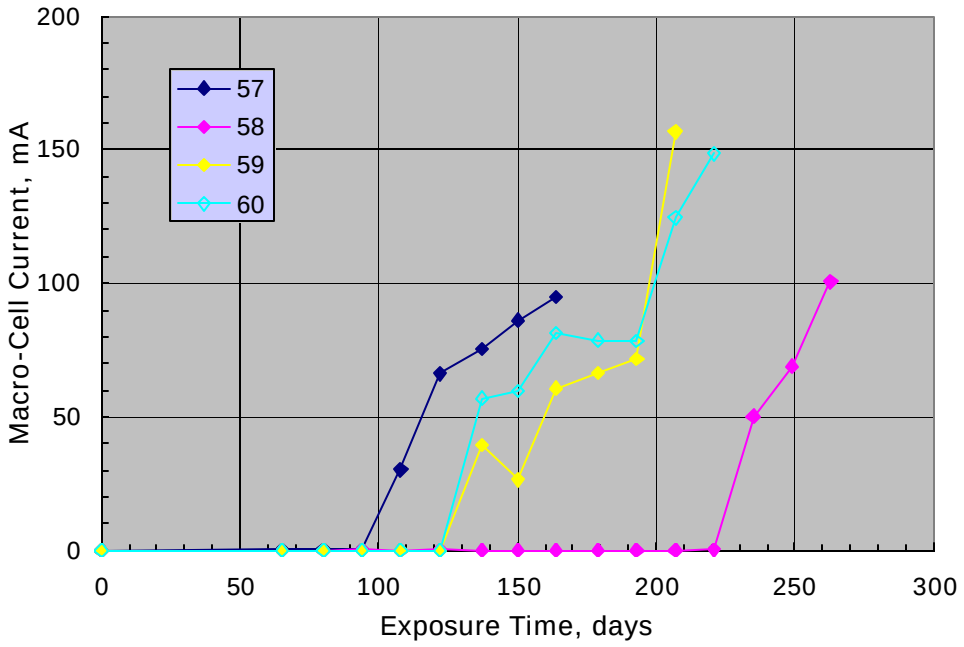

(b)

Figure 6. Potential (a) and macro-cell current data (b) for specimens of mix design LA0.50.

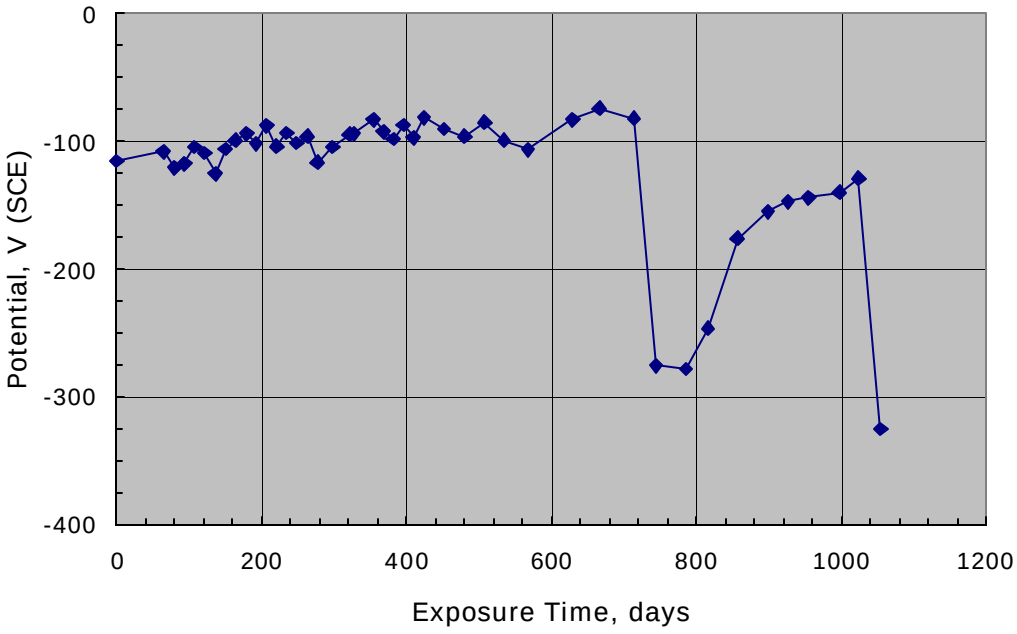

(a)

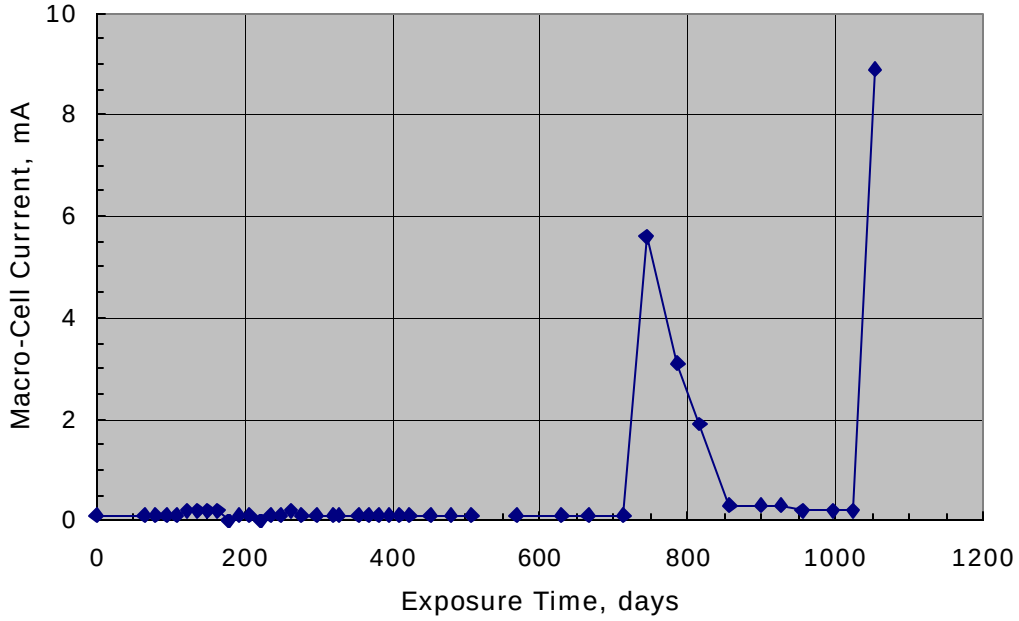

(b)

Figure 7: Potential (a) and macro-cell current (b) versus exposure time for Specimen Number 24.

Figure 8 shows the appearance of corrosion on Specimen Number 59 (LA0.50) which became active relatively early (T_i = 128 days). Termination of exposure and sectioning occurred approximately 20 days subsequent to disclosure of corrosion activity. In this case, the attack was relatively advanced, presumably because of 1) comparatively low concrete resistivity, as affected by the 0.50 w/c, and 2) the corrosion had been ongoing for several weeks. Correspondingly, Figure 9 shows a photograph of corrosion on Specimen Number 11 (HA0.41) and reveals that the extent of attack in this case was modest by comparison. Note that this latter specimen experienced a potential and macrocell current reversion subsequent to initially becoming active. For specimens in the second category, corrosion was considered to have initiated at the time when potential first dropped below –0.28 V_{SCE}, irrespective of any subsequent, more positive potential drift. Macro-cell current was often less that 10 μA at this time.

Weibull Analysis

Most commonly, experimental corrosion programs focus upon mean time-to-corrosion for a specific set of test variables. However, T_i is statistically distributed; and data thereof should be treated accordingly. For example, a bridge subjected to deicing salts may become functionally obsolete when 20 percent of the deck is delaminated or spalled. Relatedly, corrosion initiates upon substructure piers, followed by concrete cracking and spalling, according to some distribution. Unlike the bridge deck case, however, pier deterioration is more critical since achievement of a single limit state constitutes closure or failure of the entire structure. Of particular concern in the latter case are situations where the distribution has a relatively large standard deviation. Here, the average or typical degree of distress may be modest; but the deterioration state of the initially corroded one may be advanced.

Weibull anslysis is a commonly employed engineering and scientific tool for representing and projecting failures, even when relatively small samples are involved. The two parameter Weibull distribution is characterized by the expression,

$$F(T) = 1 - e^{-\left(\frac{T}{?}\right)^{ß}}, \qquad (14$$

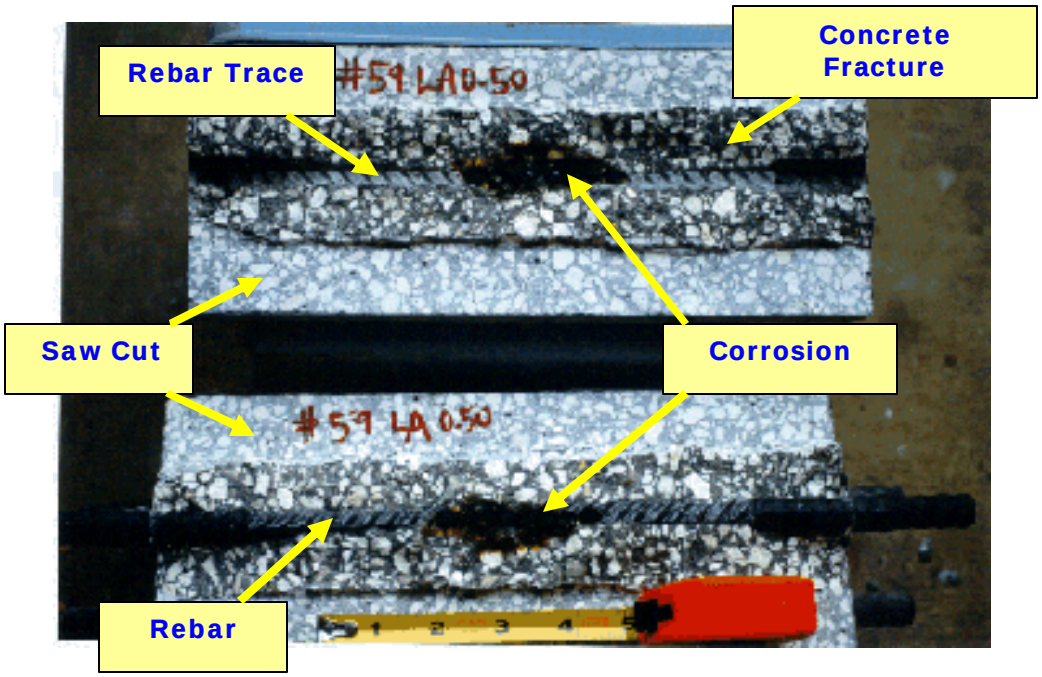

Figure 8: Photograph of section halves of Specimen Number 59 (LA0.50) showing severe localized corrosion near the center of the rebar length.

Figure 9: Sectioned view of Specimen 11-HA 0.41 showing corrosion on the upper half of the top (anodic) bar and corrosion products on the bar trace.

where

$F(T)$ = the cumulative distribution function (CDF) of the failed (corroded) fraction,

T = failure time (T_i in the present analysis),

b = the slope or shape parameter, and

h = characteristic life or scale parameter (time at which 63.2 percent of the population fails (corrodes).

The mean time to failure, T_m, is related to h by the expression,

$$T_m = ? \cdot G\left(1 + \frac{1}{ß}\right), \qquad (15$$

where $G(\bullet)$ is the gamma function. On the other hand, the value for b can infer mechanistic information. Thus, b < 1 indicates "infant mortality" or early-age failures as can occur as a consequence of manufacturing defects. An example in this category could be concrete which exhibits cracks at the time of construction such that chlorides have rapid, early access to the reinforcement. Situations where b = 1 constitute random (time independent) failures, whereas failures with b > 1 are indicative of wear-out. A critical, non-redundant component, the failure of which is characterized by a small b, is of particular concern. As an example, the initial pier to fail on a bridge with 100 piers, 50 years mean time-to-failure, and b = 1 is projected to occur after approximately eight months. However, if b = 4, the initial failure occurs at year 17.

An additional advantageous feature of Weibull analysis is that it incorporates run-outs, termed "suspensions" (specimens for which corrosion has not yet initiated in the present case).

The data in Table 4 for specimen groups that exhibited at least one incident of active corrosion were represented using the two-parameter Weibull analysis. Thus, Figures 10-12 show CDF plots for mix designs of each of the three cement alkalinities and w/c = 0.50, 0.41, and 0.37, respectively. Values for h, b, the coefficient of determination (r^2), the total number of specimens in each group (n, four in all

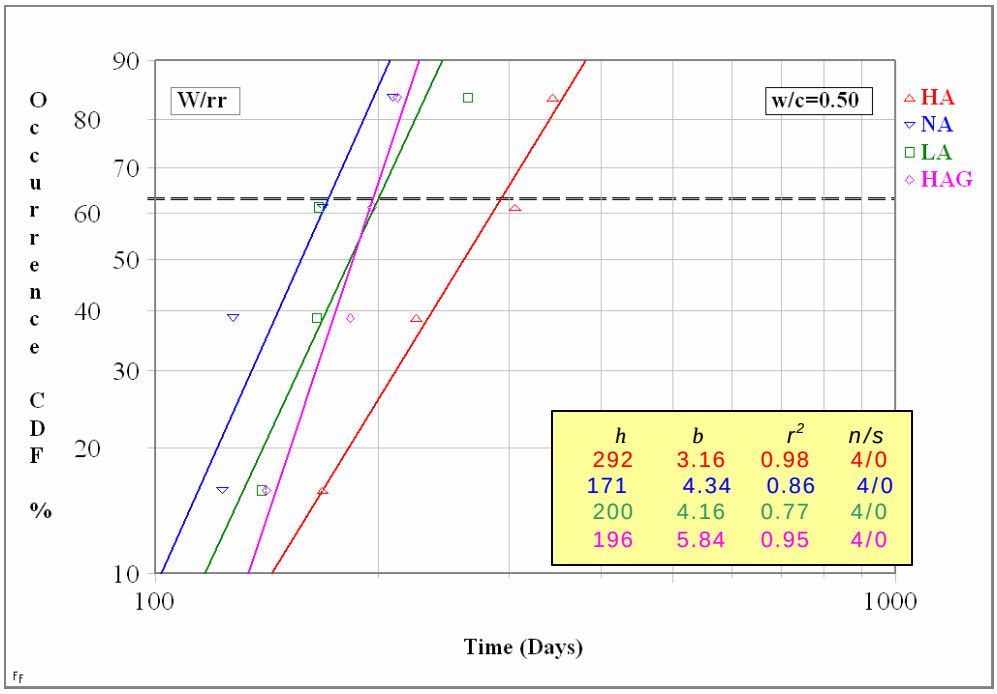

Figure 10: Two-parameter Weibull distribution of the T_i data for specimens of the 0.50 mix design.

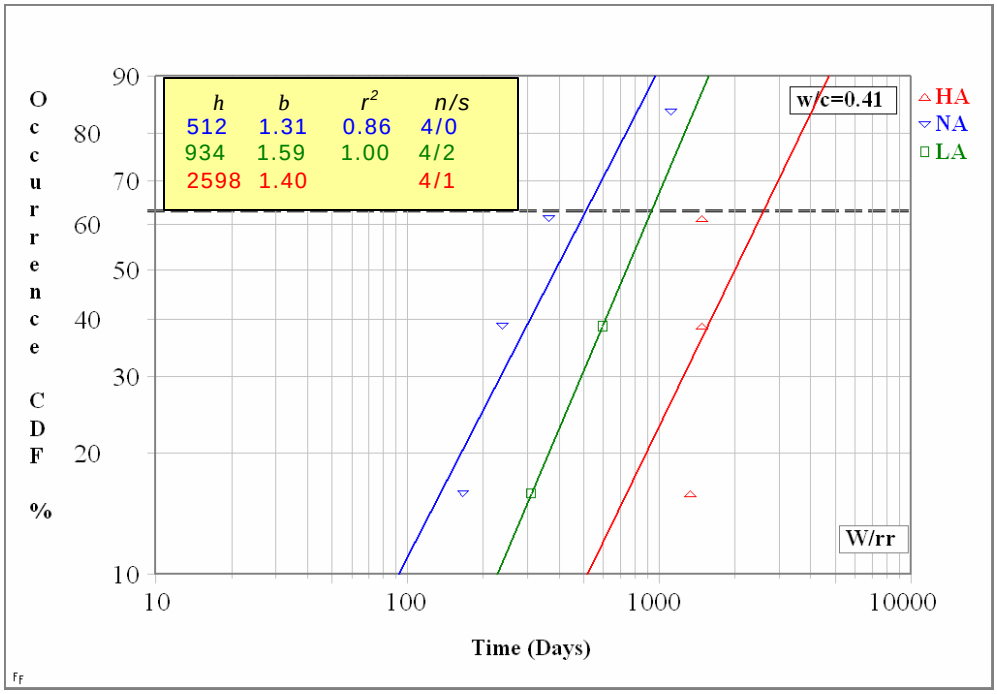

Figure 11: Two-parameter Weibull distribution of the T_i data for specimens of the 0.41 mix design. Beta for the HA data (1.40) was forced as average for the other two cement alkalinities.

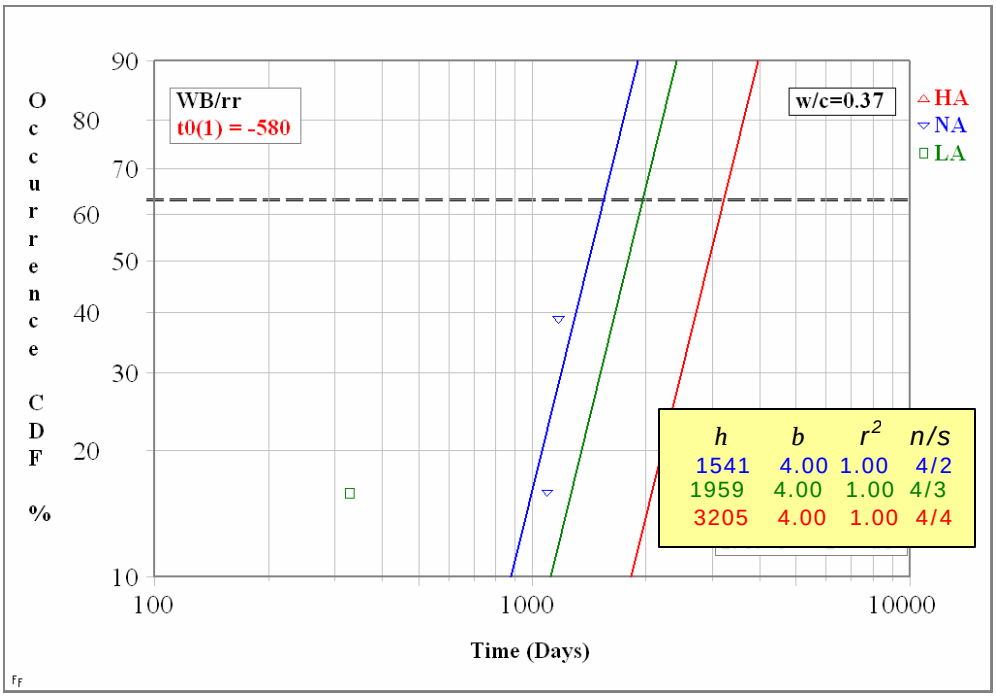

Figure 12: Two-parameter Weibull distribution of the T_i data for specimens of the 0.37 mix design. Beta values were forced as 4.00.

cases), and the number of suspensions (*s*) for each mix design are also indicated. Values for these are tabulated collectively in Table 5. Clearly, the lack of specimens for which corrosion has initiated in the lowest w/c case precludes interpretation here other than to reaffirm the beneficial effect of low w/c. In the 0.41 w/c case, *b* was forced as unity (the closest integer *b* value for NA specimens) for the LA case, where

Table 5: Listing of distribution parameters for the T_i data.

Mix Design		*h*	*b*	r^2	n/s
w/c	Alkalinity				
0.50	HAG	196	5.84	0.95	4/0
	HA	292	3.16	0.98	4/0
	NA	171	4.34	0.86	4/0
	LA	200	4.16	0.77	4/0
0.41	HA	2,598	1.40*	-‘	4/1
	NA	511	1.31	0.86	4/0
	LA	934	1.59	1.00**	4/2
0.37	HA	3,205	4.00**	-	4/4
	NA	1,541	4.00**	-	4/2
	LA	1,959	4.00**	-	4/3

* Assigned average for other two cement alkalinities.
** Beta value forced.

only one specimen has become active. Likewise, Figures 13-15 present the same data as in Figures 10-12 but according to cement alkalinity rather than w/c. These

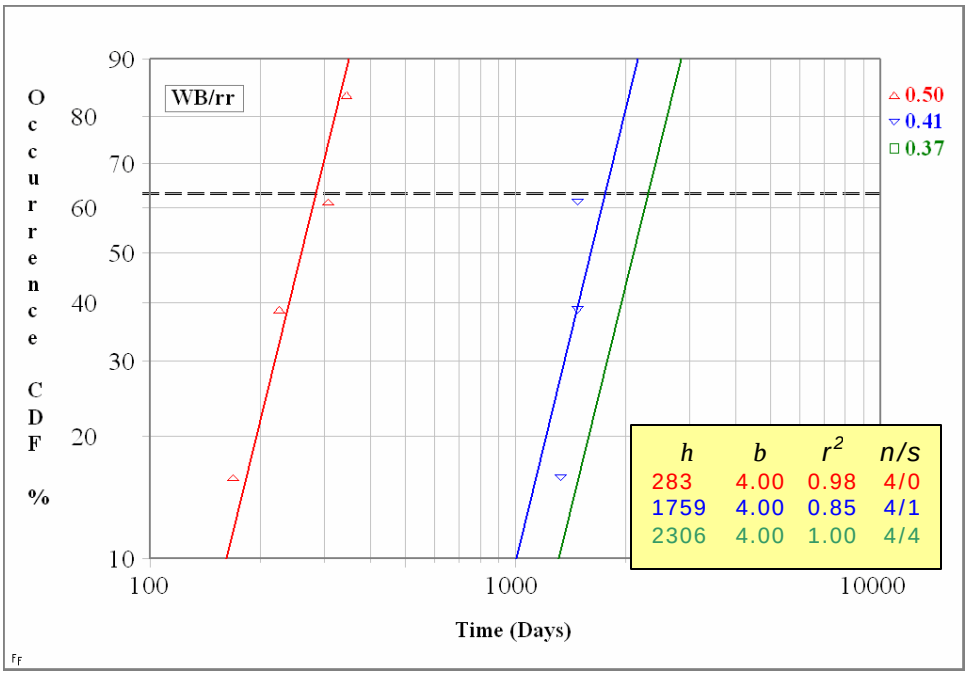

Figure 13: Two-parameter Weibull distribution of the T_i data for specimens of the HA cement. Beta values were forced as 4.00.

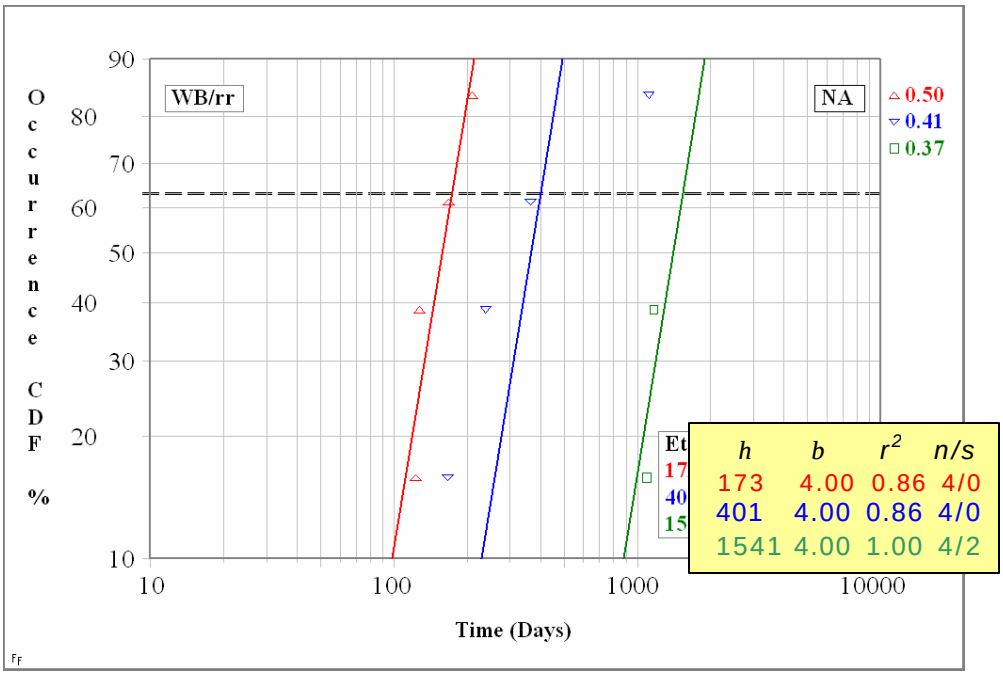

Figure 14: Two-parameter Weibull distribution of the T_i data for specimens of the NA cement. Beta values were forced as 4.00.

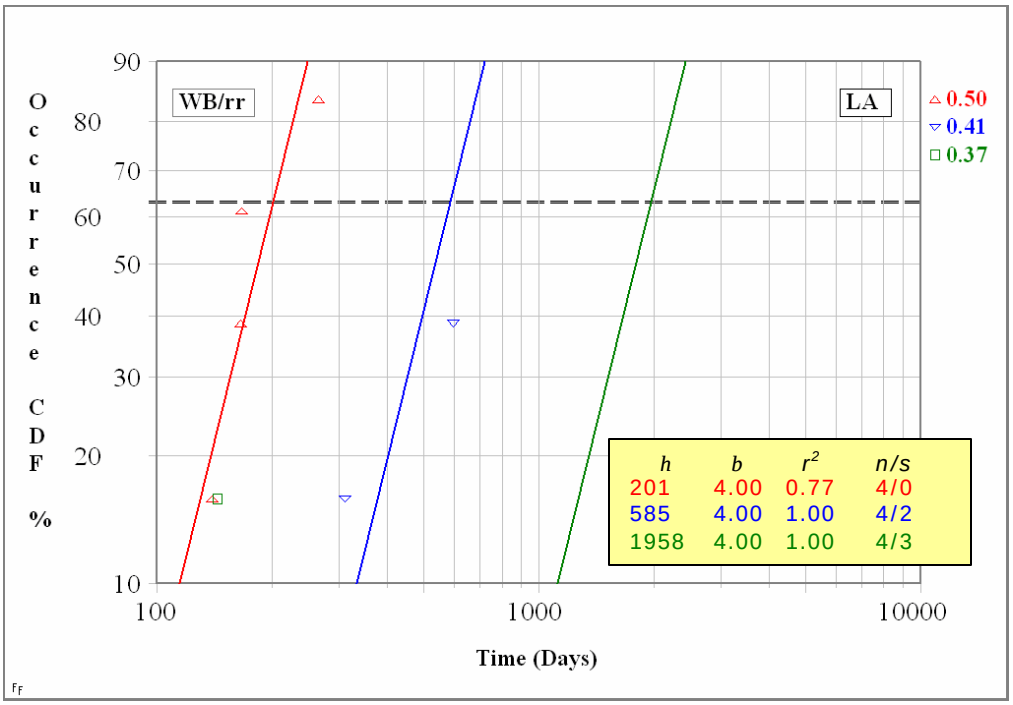

Figure 15: Two-parameter Weibull distribution of the T_i data for specimens of the LA cement. Beta values were forced as 4.00.

results indicate that, first, T_i increased with decreasing w/c, as has been documented historically by numerous investigators and, second, T_i was highest for the HA specimens. Also, h for the HA specimens with coarse aggregate was about 32 percent greater than for the HAG specimens (no course aggregate) (Figure 10). This is consistent with the inhibiting effect of coarse aggregate upon Cl^- intrusion, as reported in a companion study (25). A generalized trend of increasing T_i with increasing cement alkalinity was not disclosed, however, since for each w/c, h was greater for the LA specimens than for the NA.

Eta values, including projections where no specimens have yet become active, are shown as a function of cement alkalinity in Figure 16. Again, caution must be exercised with regard to interpretation because of the limited number of specimens that have become active; however, based upon these results, T_i for the HA specimens exceeded that for the NA and LA by a factor or 1.7-5.1.

The finding that h for the LA mix design exceeded that of the NA ones may relate to reduced Cl^- binding with increasing OH^- over the pore water pH range that applies here. In this regard, it has been reported that, because of this effect, a

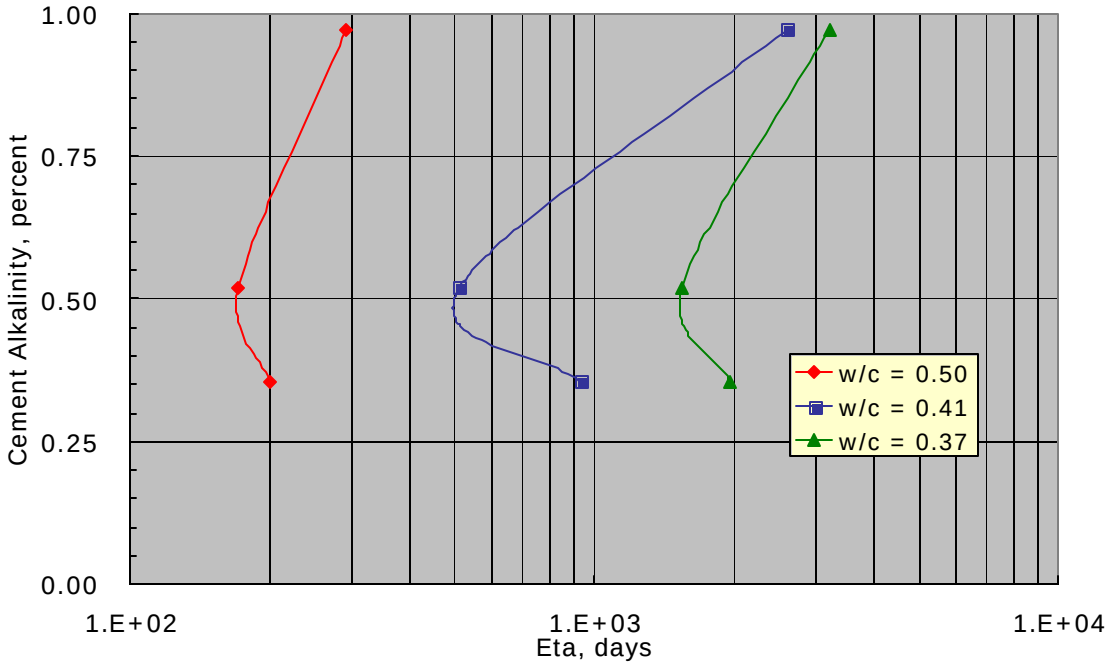

Figure 16: Plot of the eta versus cement alkalinity data.

decrease in pH at a fixed Cl^- concentration can result in an decrease in Cl^--to-OH^- ratio (26,27).

Pore Water pH

Results of the concrete porosity determinations based on water absorption capacity are shown in Figure 17. These data indicate that porosity increased with increasing w/c but was not significantly affected by cement alkalinity. The two concretes containing fly ash (NAF0.37 and NAF0.41) did not yield a lower porosity than the comparable non-admixed concretes (NA0.37 and NA0.41). This may be due to insufficient concrete curing in a highly humid environment.

Figure 18 shows the measured pore water [OH^-] for the various concrete mixes and indicates that this parameter was not sensitive to w/c. However, pore water [OH^-] increased with increasing cement alkalinity. Figure 19 plots these same results in terms of cement equivalent alkalinity. The data indicate that the average pore water [OH^-] was approximately 0.17 M for the LA concrete, 0.25 M for the NA, and 0.55M for HA.

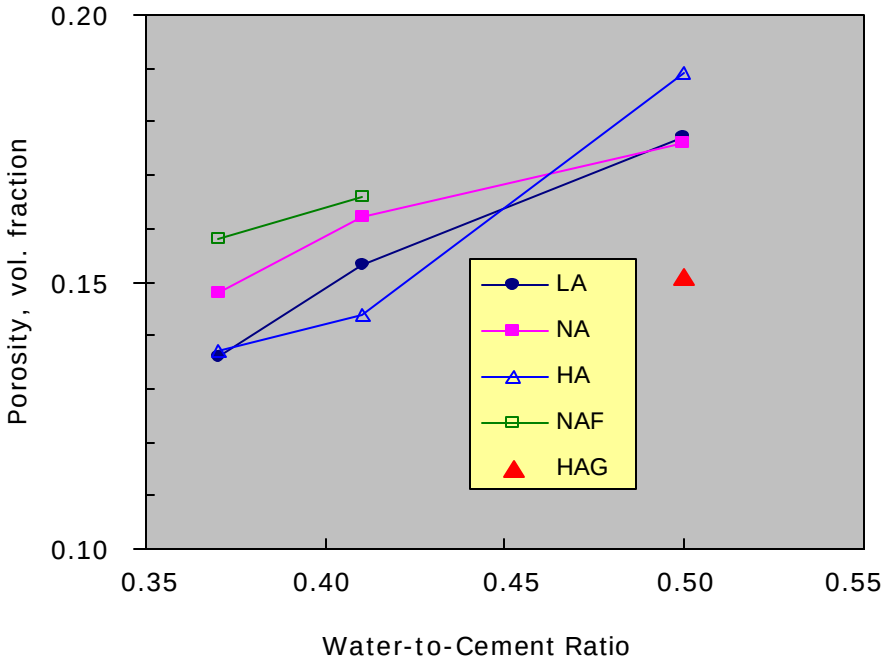

Figure 17: Plot of concrete porosity versus w/c for specimens of the different mix designs.

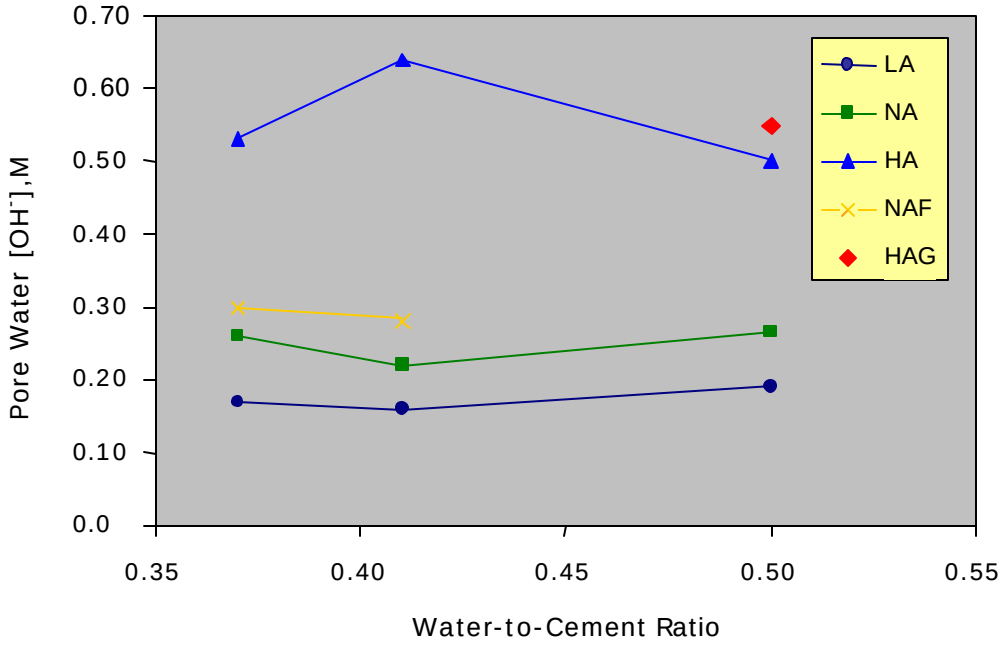

Figure 18: Pore water [OH^-] for the different concrete mixes as a function of w/c.

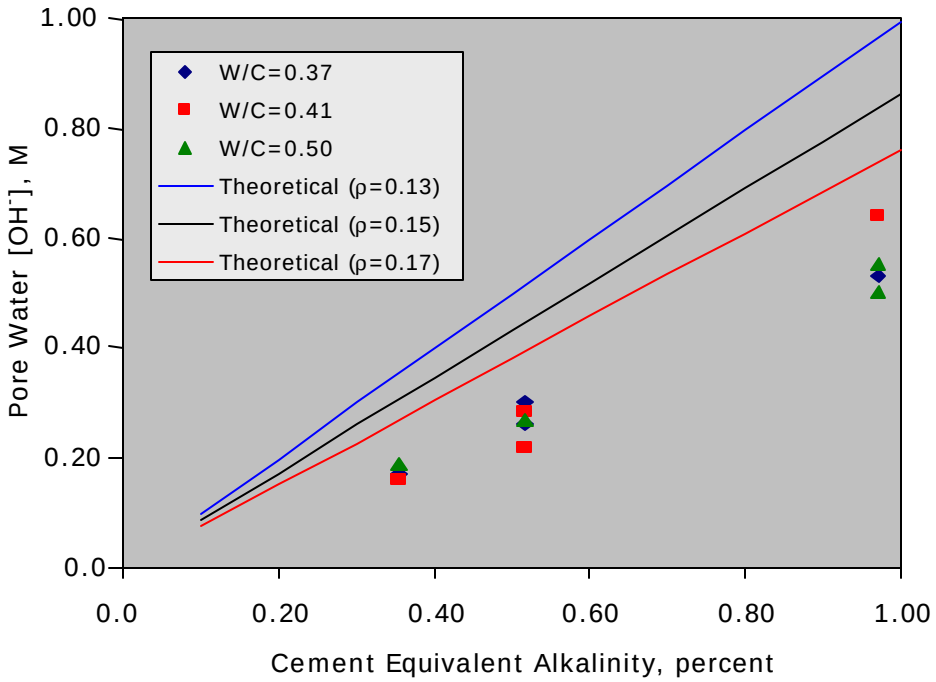

Figure 19: Effect of cement alkalinity on pore water pH (theoretical pore water [OH^-] lines are also shown).

As noted above, the high pH of concrete pore water is a result of the release to alkali ions during cement hydration. Stochiometrically, the reaction of each mole of cement alkali oxide produces two moles of hydroxide. Therefore, the theoretical [OH^-] in the concrete pore water is,

$$[OH^-] = \frac{C \cdot EqA \cdot r}{50 \cdot MW \cdot ?}, \qquad (16$$

where

C is the cement content of a concrete mix (kg/m^3),

r is the degree of cement of hydration (fraction), and

MW is the molecular weight of Na_2O (gms/mol).

Theoretical [OH^-] values for concrete with C= 400 Kg/m^3, r=1.00, and ρ=0.13, 0.15, or 0.17 are plotted as lines in Figure 19. These lie above the measured values, suggesting that full cement hydration had not been achieved with even the powdered concrete samples exposed to distilled water for three days. It cannot be discounted, however, that the OH^- exhibited a binding effect similar to that of chlorides in concrete. The data indicate that [OH^-] for the HA mix concrete was approximately

twice that of the NA, the latter being typical of Florida practice. Thus, the ratio of $[Cl^-]$-to-$[OH^-]$ for concretes of each of these two mixes that were similar except for cement alkalinity and which underwent identical exposure should, for the HA mix concrete, be approximately one-half that of the NA. If this ratio alone governs the onset of passive film breakdown and active corrosion, then Cl^- tolerance for the HA concrete should be twice that of the NA. However, the data in Figure 17, where h was greater for the LA concrete than for the NA, indicates that one or more other factors was also involved as noted above.

Figure 20 compares the present $[OH^-]$ versus *EqA* results with ones available from the literature. This indicates relatively good agreement between the two with the present data occupying the lower bound of the results by others.

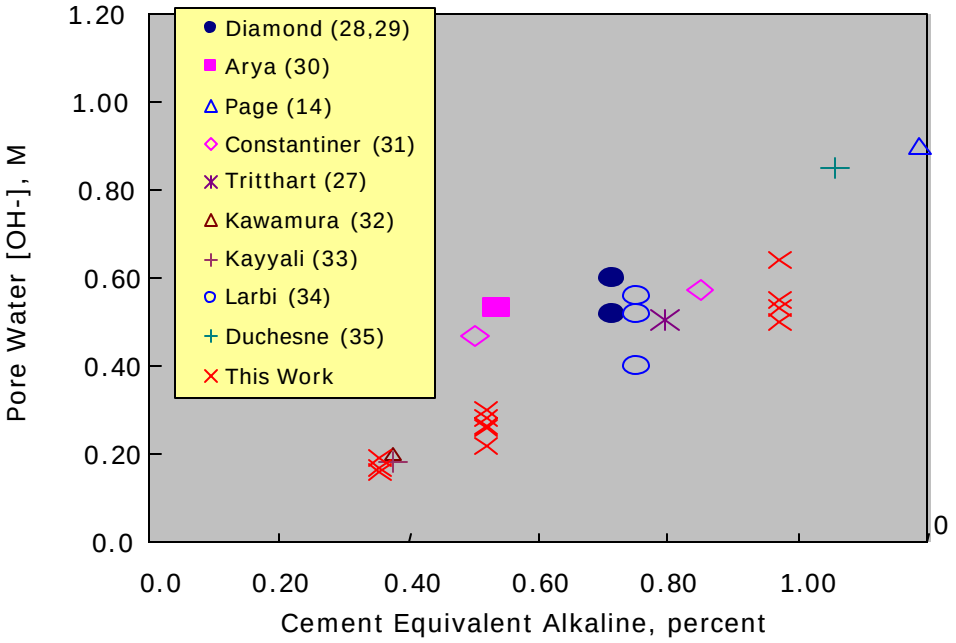

Figure 20: Relationship between pore water $[OH^-]$ and cement equivalent alkalinity as determined in the present and by past research.

Figure 21 plots the results from Figure 20 on the basis of pH and shows that this parameter ranged from 13.05 to 13.20 for the LA mix, 13.19 to 13.36 for the NA, and 13.53 to 13.65 for the HA.

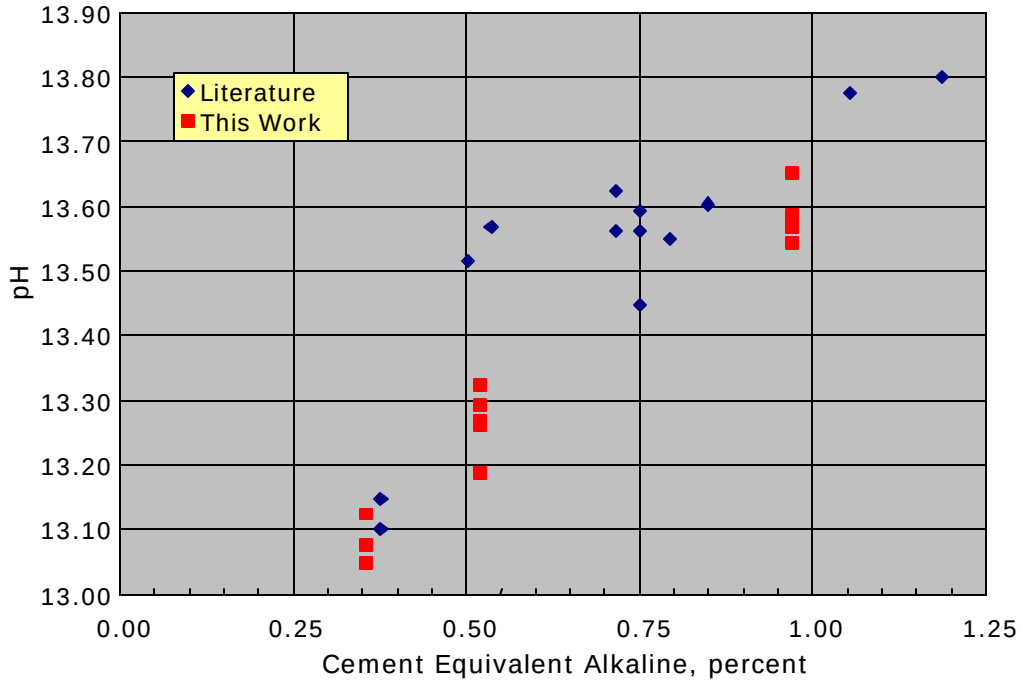

Figure 21: Relationship between pore water pH and cement equivalent alkalinity as determined in the present and by past research.

Chloride Analysis Results

Diffusion Coefficients

Figure 22 illustrates typical acid soluble [Cl^-] analysis data as a function of distance beneath the ponded concrete surface, as determined from a core acquired from four of the blank (non-reinforced) specimens after 1,616 days of cyclic ponding exposure. These results provide some insight into specimen-to-specimen scatter (HA specimens), and indicate less Cl^- penetration for this mix compared to the lower equivalent alkalinity ones. Likewise, Figure 23 presents a plot of D_{eff} versus *EqA* with the data partitioned according to w/c. Cores from which the samples were acquired for the D_{eff} determinations were taken at either 1,210 or 1,616 days exposure except for the single 0.50 datum for which this time was 133 days. The data indicate that D_{eff} for *EqA* = 0.97 was lower than for 0.52 by 44 percent. Figure 24 compares the average D_{eff} results from the present study with ones available from the literature (30) and indicates that the present values are relatively high in comparison.

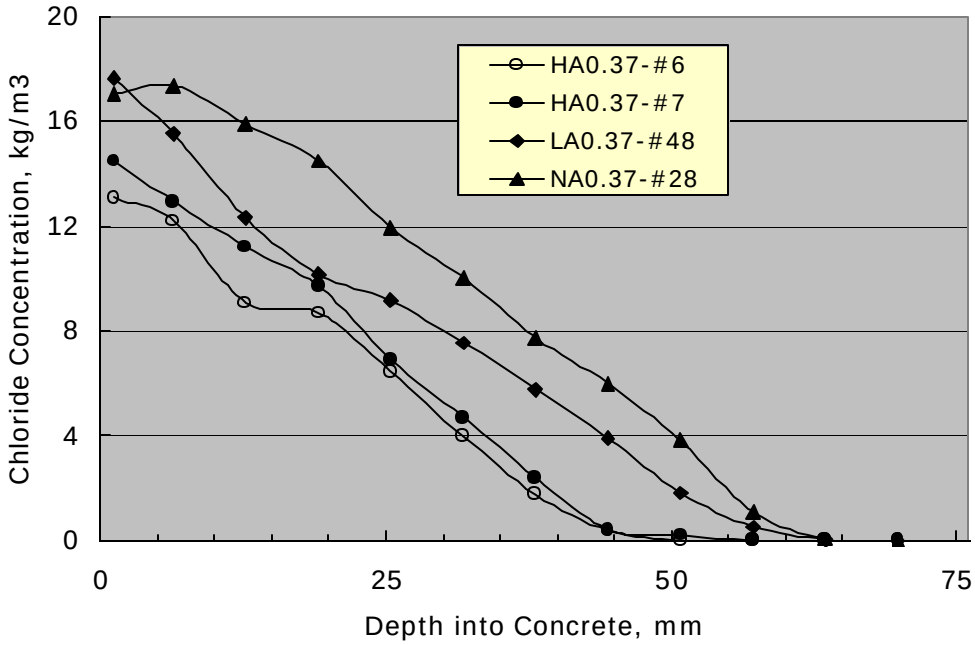

Figure 22: Example acid soluble [Cl^-] data as a function of distance beneath the ponded concrete surface.

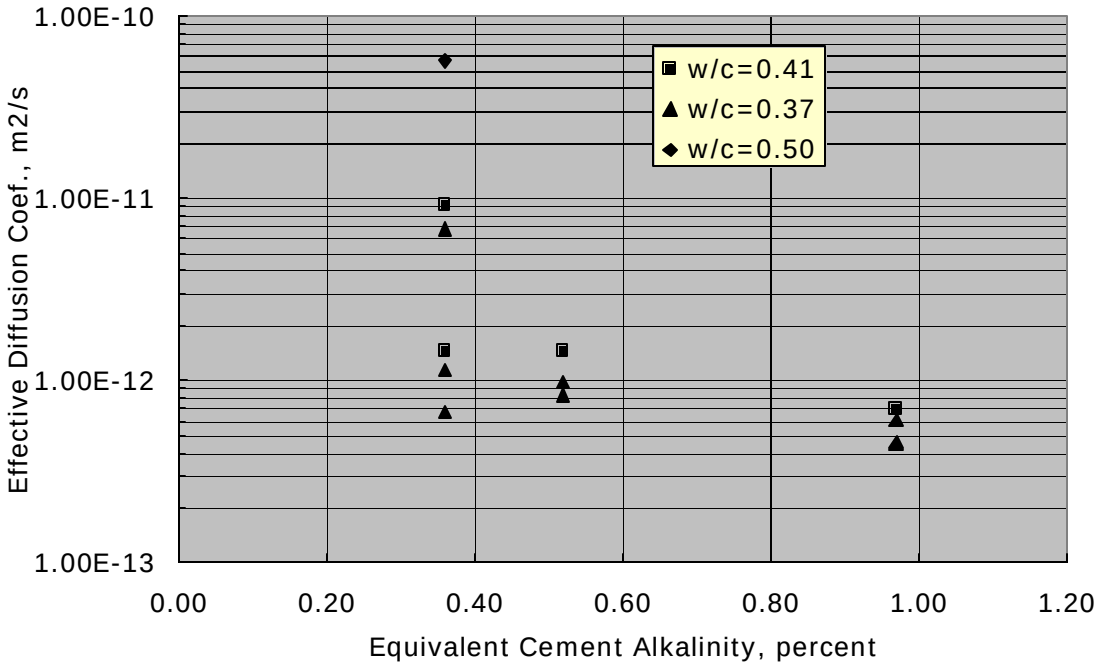

Figure 23: Effective diffusion coefficient data as a function of equivalent cement alkalinity.

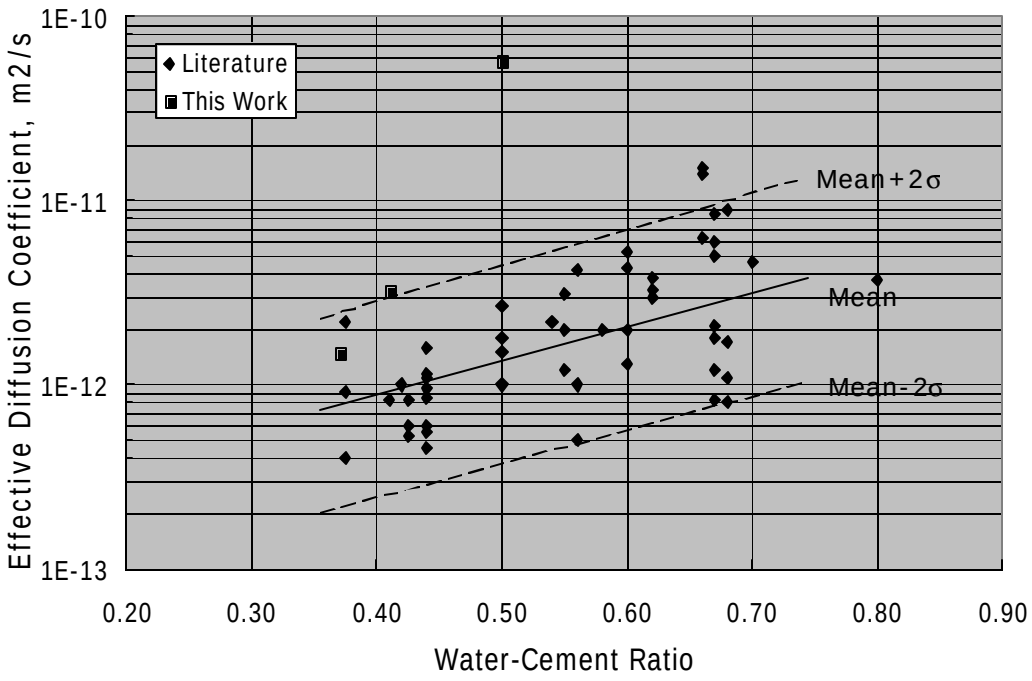

Figure 24: Comparison of D_{eff} values from the present specimens with those reported from the literature.

Figure 25 shows the Cl^- profile that was determined for a core taken from a previously tested LA0.50 specimen that was inverted approximately 50 months after casting and re-ponded on what was initially the bottom surface for a single wet-dry cycle. Also shown are profiles for LA0.41 and LA0.37 specimens (no LA0.50 specimen was available) after 80 wet-dry ponding cycles. Irrespective of the fact that specimens of different w/c are involved, the profile for the one-cycle specimen indicates that considerable Cl^- uptake occurred early in the exposure, presumably as a consequence of sorption. Thus, sorption could have been responsible for or contributed to the relatively high D_{eff} values that were calculated for the present specimens (see Figure 24). The fact that sorption affected the $[Cl^-]$ profiles brings into question the appropriateness of data analysis based upon Fick's second law.

Chloride Threshold Concentrations

Table 6 lists $[Cl^-]$ values that were measured for powdered concrete samples acquired from the top region of the upper rebar trace of specimens that had become active, both at the active corrosion site and elsewhere where the steel remained passive. Also listed are T_i and the exposure time at which the specimens were

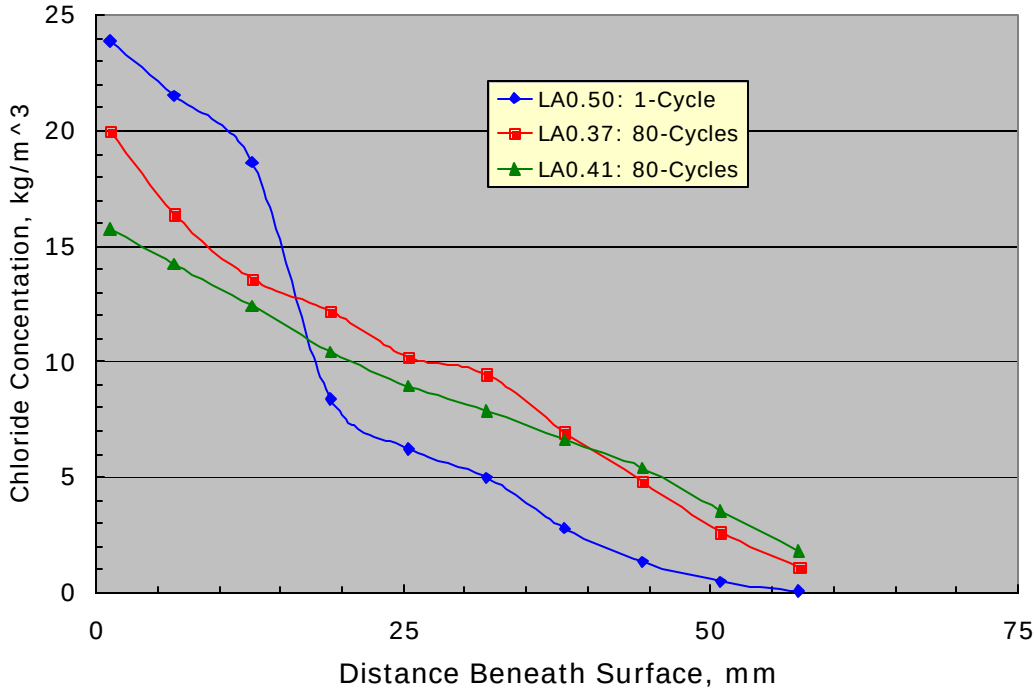

Figure 25: Chloride profile after one wet-dry cycle compared to after 80 cycles.

autopsied. From these times and the D_{eff} values (Table 7), [Cl^-] at time T_i was back-calculated; and this value was taken as c_{th}. Figure 26 shows a plot of c_{th} versus T_i and indicates that in most cases [Cl^-] at the active corrosion site exceeded that where the steel remained passive. However, in most of the cases where specimen autopsy was performed at the time when potential first became negative to -0.28 V_{SCE}, [Cl^-] at the active and passive sites was approximately the same. This suggests that the elevated [Cl^-] at the corrosion site resulted from electromigration subsequent to corrosion initiation. If this was the case, then it is the remote site [Cl^-] that should be taken as c_{th}. No explanation is available for the data from Specimen 11-HA0.41, which is an exception to this trend. The general trend in Table 6 and Figure 26 is one where c_{th} increased with time, albeit at an ever decreasing rate, irrespective of mix design. Thus, while specimens of the normal and low cement alkalinity and high w/c exhibited the shortest T_i and vise versa, all data conformed to a common trend. This is consistent with, first, chlorides having continued to progressively accumulate with increasing time and, second, T_i being a distributed parameter, as discussed above.

As noted above, c_{th} values in the range 0.60-0.75 kg/m^3 (1.0-1.3 pcy) have

Table 6: Exposure time data for specimens that have become active.

Specimen Number	$[Cl^-]$, kg/m^3 (Active)	$[Cl^-]$, kg/m^3 (Passive)	Time-to-Corrosion, days	Total Exposure Time, days
15 - HA 0.50	11.98	8.92	136	211
16 - HA 0.50	15.39	10.59	297	324
17 - HA 0.50	18.28	11.32	391	433
18 - HA 0.50	12.54	10.92	255	319
10 - HA0.41	23.27	23.53	1,192	1,459
11 -HA0.41	33.50	16.82	1,401	1,455
24 - NA0.37	10.93	10.76	1,096	1,124
25 - NA0.37	27.64	-	1,192	1,229
29 - NA 0.41	15.63	7.92	136	211
30 - NA 0.41	15.18	12.86	206	256
31 - NA 0.41	17.39	14.41	339	381
32 - NA0.41	18.76	-	1,120	1,186
36 - NA 0.50	19.67	10.93	93	183
37 - NA 0.50	19.56	6.90	93	213
38 - NA 0.50	16.62	9.13	136	256
39 - NA 0.50	10.22	7.29	178	211
45 - LA 0.37	16.90	11.22	149	211
50 - LA 0.41	10.44	10.95	297	324
52 - LA 0.41	21.46	16.49	567	576
58 - LA 0.50	11.87	5.42	234	264
59 - LA 0.50	15.61	4.31	136	211
60 - LA 0.50	20.33	7.37	136	256
64 - HAG 0.50	8.70	7.59	149	190
65 - HAG 0.50	7.84	6.87	178	211
66 - HAG 0.50	11.64	7.84	107	217
67 - HAG 0.50	13.99	9.18	163	211

historically been reported (1,2) from North America bridge deterioration deck studies. Consistent with the projection above that c_{th} is a function of multiple factors, as well as being statistically distributed, Glass and Buenfeld (9) reported values in the range 0.17-2.5 (total Cl^- on a cement w/o basis) based upon literature data. This translates to 0.66-9.71 kg/m^3 (concrete weight basis) for the cement content of the present specimens (Table 2). This upper limit from the Glass and Buenfeld summary approximates the mid-value determined from the present exposures. Possible explanations for the present relatively high c_{th} values include the following:

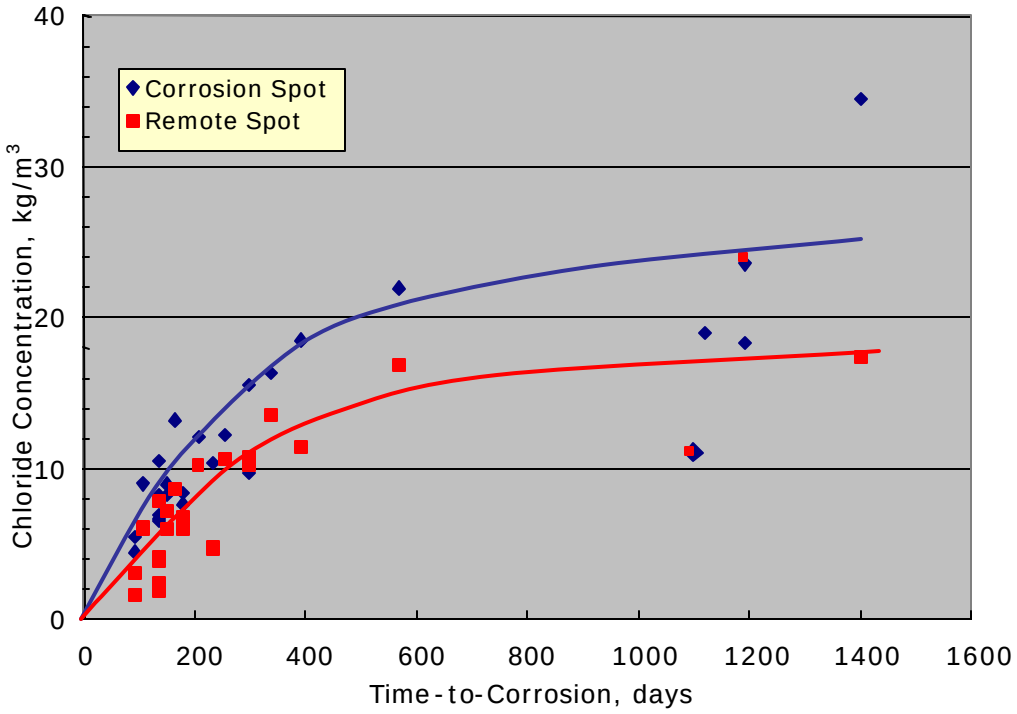

Figure 26: Plot of Time-to-Corrosion as a function of [Cl^-] for specimens that have become active.

1. Specimens were exposed in laboratory air at a constant relative humidity (RH) of about 70 percent.

2. The absence of RH and temperature variations.

3. Chloride binding effects.

4. Surface condition of the reinforcement (wire brushed as opposed to as-received).

5. The passive film upon the steel may become more stable with time.

6. Concrete aging with time.

7. Specimens were relatively small such that the nature of the steel-concrete interfacial may not reflect statistically the variability that can arise in large structures.

With regard to Items 1 and 2, it can be reasoned that temperature/relative humidity variations, as occur with outdoor conditions, promote fluxes of moisture and oxygen

in concrete that do not take place under controlled laboratory conditions and that these, in turn, facilitate the onset of corrosion. Experiments are ongoing to investigate this further.

Chloride binding (Item 3) reduces the concentration of this species that is "free" and, hence, available to participate in steel depassivation and corrosion. While it is reasonable to assume that some fraction of the total chlorides that migrated into the concrete specimens became bound, it is unlikely that the concentration of these was sufficient to account for the difference between the measured c_{th} for the present experiments (4.3-23.5 kg/m^3 (7.3-39.5 pcy), see Table 8) compared to historically reported values for North America bridge concretes (1,2), given that, first, this difference is by a factor of 7-40 and, second, C3A concentration for all three cements was in the normal range (see Table 1).

Li and Sagüés (8) found, based upon exposure of carbon steel in simulated pore water solutions (pH ~ 12.6-13.6), that c_{th} for as-received and pre-rusted specimens was approximately twice that of sandblasted ones. If performance of specimens with a wire brushed surface finish, as was the case for the present experiments, is comparable to sandblasted and if results from aqueous exposures can be quantitatively compared to those for steel in concrete, then this factor (surface preparation) probably contributed to about a factor of two of the difference between the present and previously reported (1,2,9) c_{th} values.

Items 5 and 6 were addressed by a series of experiments where the G109 specimens that had become active were retested. This involved reconfiguring these by inverting, grouting together the split specimen halves, reponding, and monitoring potential of what was, upon initial exposure, the two bottom bars for onset of active corrosion. The regrouting was intended to provide mechanical stability to the specimens, and no electrical connection was made between the top and bottom bars. Figure 28 shows a photograph of two of these specimens. The specimens were originally fabricated over a one month period in late-1997, and the original ponding commenced in July, 1998 (approximate concrete age eight months). The reponding, on the other hand, began in June, 2001 (approximate concrete age 43 months). It was reasoned that if either enhanced passivity with time or concrete aging caused or contributed to the observed c_{th} versus time trend, then the results upon reponding

Figure 27: Photograph of two repaired and inverted specimens under test.

should exhibit greater T_i and c_{th} than occurred upon the initial exposure.

Figure 28 presents the Weibull formatted T_i results upon reponding for the HA0.50 specimens in comparison to data for the original exposures. Here, the b value for the two data sets is approximately the same; however, h was less for the reponded tests than for the originals by a factor of approximately three. Results for the NA0.50 and LA0.50 specimens were similar, although in these cases the difference in h was by a factor of 1.8 and 2.5, respectively. On the other hand, h for the reponded HAG specimens was slightly greater than for the original tests. The relatively small number of NA0.41 and LA0.41 specimens in either category (original or retest) that have become active precluded realistic comparisons here, although the limited results are consistent with h being less for the reponded exposures. On this basis, Items 5 and 6 were both discounted as being possible explanations for the relatively high c_{th} values and the variation with time.

With regard to Item 7 (size effect), it is generally recognized in failure analysis that the probability of failure increases with increasing member size. When mechanical fracture is involved, a contributing factor is that strength often decreases with increasing section thickness because of fabrication effects. Also at issue is the fact that the probability of a critical size defect being present increases with increasing size. On this basis, a relatively small G109 specimen is less likely to

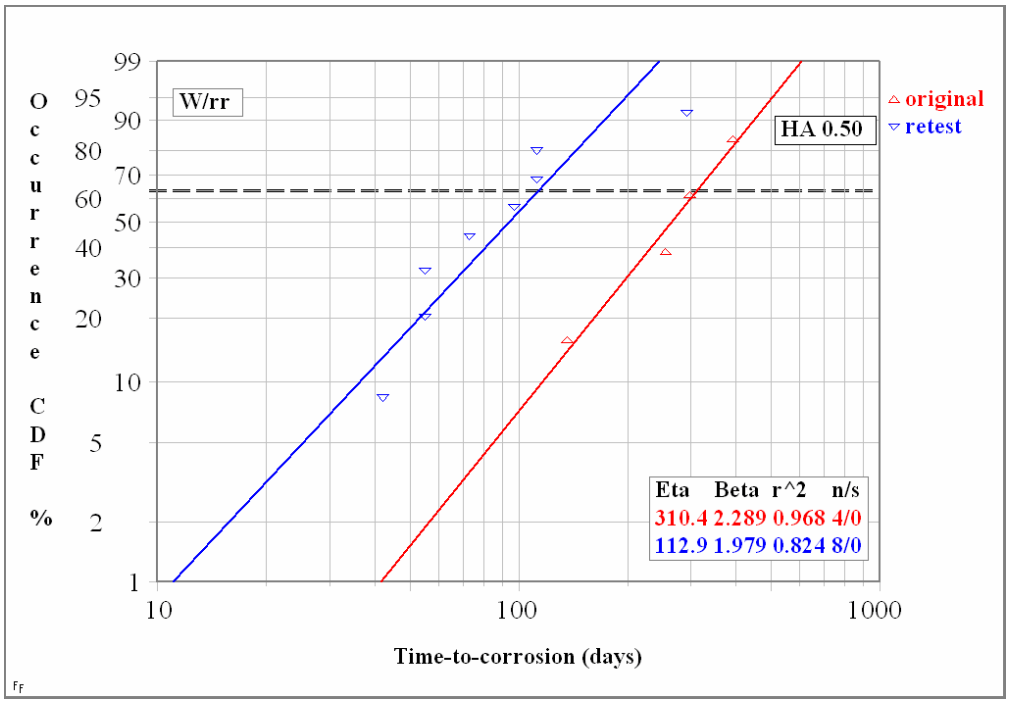

Figure 28: Weibull distributions of T_i for the original and retested exposures of HA0.50 specimens.

exhibit a corrosion initiating feature or defect of a specific significance than is a large slab or structure. Exactly what type of defect(s) or microstructural feature(s) could serve such a role in the case of reinforcing steel in concrete is uncertain; but possibilities include 1) the heterogeneous nature of concrete such that some specific condition is locally established at the steel-concrete interface, 2) a preexisting geometrical feature upon the steel surface (locally severe surface roughness or a micro-crevice, for example), and 3) a pit-promoting microstructural feature at the steel surface (inclusions, for example). No effort was made to investigate 2) and 3); however, as a matter of hindsight, it was possible to discern information that may pertain to 1).

Previous research has reported that corrosion of reinforcing steel preferentially initiates at concrete voids that impinge upon the steel (37). Visual observation of the initial specimens that became active in the present project revealed one or more air voids at the site of active corrosion. Figure 29 shows an example of this for Specimen 59 (LA0.50). Any such voids at the corrosion site of specimens that became active later were not detected because of the build-up of corrosion products here. Further into the program, however, the question of corrosion initiating at voids

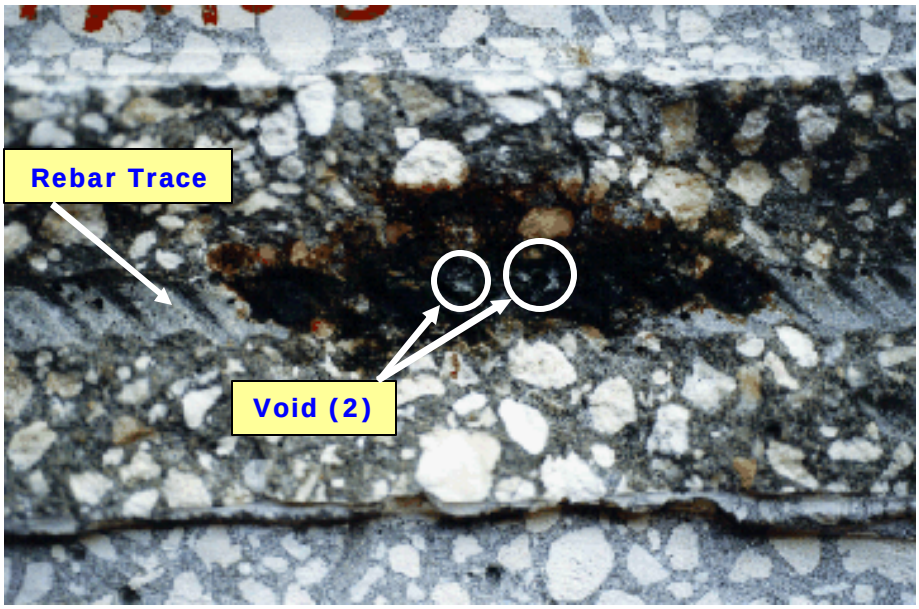

Figure 29: Photograph of rebar trace at the active corrosion site for Specimen 59 (LA0.50) after autopsy showing concrete voids at or near the corrosion epicenter.

in the concrete was revisited. In this regard, Figure 30 shows a general view of Specimen 10 (NA0.41) subsequent to sectioning; and Figure 31 presents a close-up photograph of the corrosion site that was taken shortly after sectioning. Deliquescent droplets that are apparently hydrolyzed corrosion products of low pH are apparent here. Figure 32 shows a close-up view of the rebar trace in the concrete at the corrosion site opposite the view in Figure 31. This reveals a void in the concrete at the corrosion site (circled area) corresponding to a location of deliquescence in Figure 31.

Specimen 10 was sectioned further, and the rebar trace at the corrosion site was viewed using a scanning electron microscope and chemically analyzed via Energy Dispersive X-ray Diffraction (EDX). In this regard, Figure 33 reproduces Figure 32 with various void areas that were analyzed identified. Correspondingly, Table 7 lists the chlorine, presumable as Cl^-, analysis results for these and shows that this species was present at almost 22 w/o at the void where corrosion had initiated. This high value presumably resulted from electromigration, as discussed above. Such a concentration is consistent with the deliquescent nature of the corrosion products. The average [Cl^-] for the other voids was approximately one w/o. Even this is a

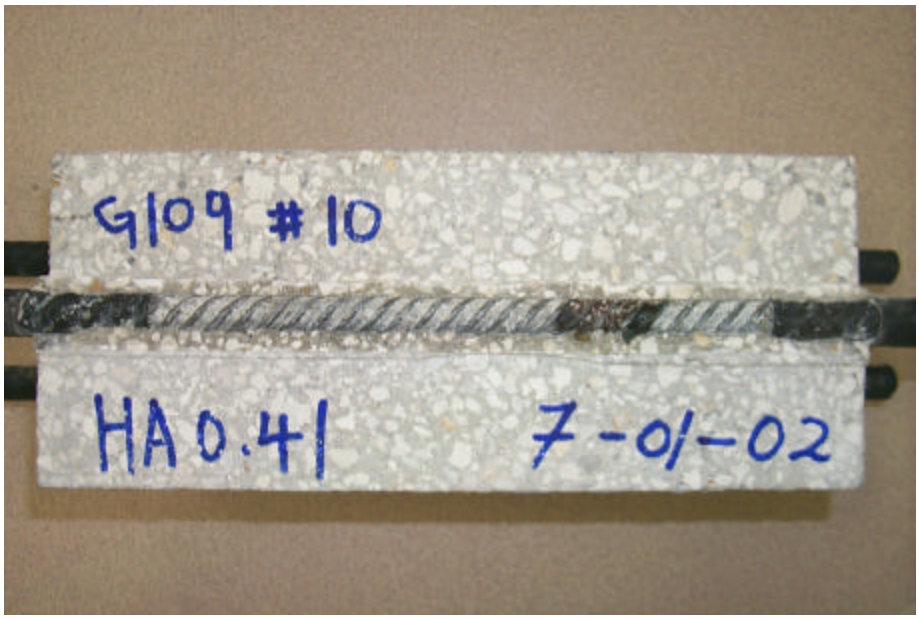

Figure 30: Photograph of Specimen 10 (HA0.41) after sectioning showing active localized corrosion on the upper portion of the top bar.

Figure 31: Photograph of the locally corroded region on the exposed top half of the upper rebar of Specimen 10 (HA0.41) after sectioning.

relatively high value and may reflect a tendency for chlorides to concentrate at voids or the relatively poor accuracy of EDX at low concentrations. It was not possible to analyze other specimens in a similar fashion because powder drilling had already been acquired from the corrosion site on these.

Figure 32 Close-up view of the rebar trace in the concrete at the corrosion site of Specimen 10 (HA0.41).

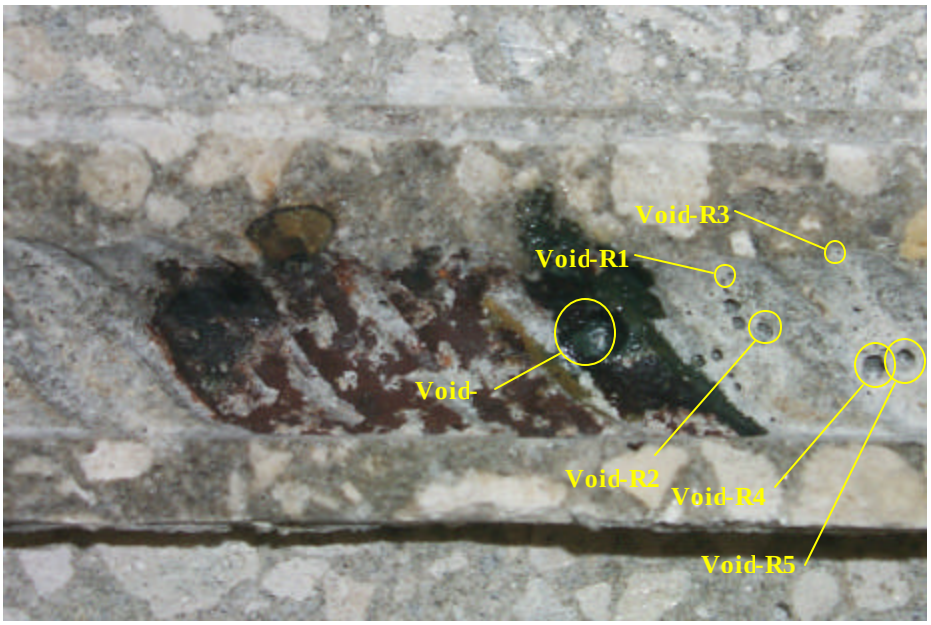

Figure 33: Photograph of the rebar trace from Specimen 10 (HA0.41) showing concrete voids that were compositionally analyzed.

Table 7: Chloride analysis results for the voids identified in Figure 34.

Location					
Void-C	Void-R1	Void-R2	Void-R3	Void-R4	Void-R5
21.88	1.43	0.66	-	0.93	1.87

Based upon the above observations, it is concluded that concrete voids may have facilitated passive film breakdown and onset of localized corrosion for the present specimens. If this was the case, then the mechanism probably involved a concentration cell with contiguous concrete coated and bare steel serving as cathode and anode, respectively. In this regard, it has previously been reported (38) that such a cell has a relatively high driving potential and is likely to be compounded by an unfavorable surface area ratio (small anode–large cathode). It can be reasoned that the specimen of a given mix design with the largest void intersecting the top portion of the upper bar activated first and vise versa. On this basis, the variability in c_{th} (Table 8 and Figure 26) resulted in response to probabilistic aspects of void size, density, and distribution.

If voids were a factor in corrosion initiation for the present specimens, then the possibility exists that durability of concrete structures could be enhanced by any treatment that reduces their size and density. This might be affected by 1) innovative placement procedures, 2) admixtures that are specially formulated for void size/density reduction, and 3) employment of self-consolidating concrete. Additional specimens must be analyzed microscopically and additional exposures performed before definitive conclusions can be reached regarding this possibility.

ACKNOWLEDGEMENT

The authors are indebted to Mr. Rodney Powers of the FDOT Corrosion Laboratory for fabricating the specimens and to Mr. George Jones for assistance with various aspects of the experiments.

CONCLUSIONS

The following conclusions were reached based upon exposure of a series of G109 concrete specimens to cyclic wet-dry ponding with a 15 w/o NaCl solution.

1. Time-to-corrosion for “identical” specimens of each mix design varied, often over a relatively wide range. This resulted because this parameter, time-to-corrosion, is statistically distributed and is effected by a number of factors, each of which is also distributed.

2. Of the Type II cements that were employed in specimen fabrication, the exposure time for passive film breakdown and onset of active corrosion, T_i, was least for ones that that were of "normal" alkalinity (equivalent alkalinity 0.52 (designation NA)), intermediate for a "low" alkalinity cement (equivalent alkalinity 0.36 (designation LA)), and highest for "high" alkalinity (equivalent alkalinity 0.97 (designation HA)). Because the equivalent alkalinity of cements typically utilized in Florida bridge construction is comparable to that of the NA type and because alkali silica reaction is not normally a problem in the State, improved corrosion resistance can be realized using cements of the HA type. The increase in time-to-corrosion for specimens with the HA cement compared to the NA ones was by approximately a factor of three for water-cement ratio 0.37 and by a factor of ten for water-cement ratio 0.41. Time-to-corrosion did not increase monotonically with cement alkalinity in that T_i was greater for specimens with the LA cement than with the NA. This is thought to have resulted from relatively high Cl^- binding in the lower pore water pH range.

3. Pore water pH was in the range 13.05-13.20 for the LA mix concrete, 13.19-13.36 for the NA, and 13.53-13.65 for the HA. This resulted from OH^- concentration for the HA cement concrete being about a factor of two greater than for the NA. The pH-cement alkalinity trend for the present concrete mixes was slightly above the lower bound of data in the literature.

4. The threshold chloride concentration to cause passive film breakdown and active corrosion, c_{th}, increased with increasing T_i. Consequently, the HA specimens exhibited the highest c_{th} although all data conformed to a common trend. Local chloride concentrations in the concrete measured from powder drillings taken along the top side of the upper rebar trace varied from 7.84 to 27.64 kg/m^3 (concrete w/o basis) at the site of active corrosion and from 4.31 to 23.52 kg/m^3 at locations where the steel was passive. This difference presumably resulted from electromigration of Cl^- to active sites subsequent to corrosion initiation. The latter range (4.31 to 23.52 kg/m^3) is considered to represent c_{th}, since Cl^- electromigration and rapid accumulation of this species subsequent to corrosion initiation should not have occurred here. This range

(4.31 to 23.52 kg/m^3) exceeds what is typically assumed to initiate reinforcement corrosion in North American bridge deck concretes (0.60-0.75 kg/m^3 (1.0-1.3 pcy)) by a factor of 6-39. On the other hand, the general literature reports the range for c_{th} as 0.66-9.71 kg/m^3 which, while overlapping, is still less than determined for the present specimens.

5. The effective diffusion coefficient, D_{eff}, increased with increasing water-cement ratio and was about 40 percent lower for concrete prepared with the HA cement compared to the NA and LA ones. The present D_{eff} values are at the upper bound or exceed those reported in the literature. Results from short-term exposures indicated that sorption was a significant contributor to Cl^- uptake by the present specimens, and this apparently inflated the D_{eff} determinations. This role of sorption also brings into question the appropriateness of Fick's second law for analyzing the present Cl^- data.

6. In situations where observations were made, corrosion was found to have initiated at a void in the concrete that impinged upon the reinforcement. A concentration cell whereby the contiguous concrete coated and bare steel served as cathode and anode, respectively, is considered to have been responsible. The size and density distribution of these voids may have contributed to or been responsible for the finding that T_i was a distributed parameter.

RECOMMENDATIONS

Based upon the results of this research it is recommended that further research be performed to determine the following:

1. Feasibility of the private sector producing high alkalinity cements suitable for Florida bridge construction. Such a study should consider a) identifications of problems that industry might encounter in accomplishing this, b) different options for attaining high alkalinity, and c) definition of an appropriate alkalinity range for corrosion resistance enhancement.
2. Confirmation of the role of air voids in corrosion initiation. Activities in this category, subsequent to confirmation, should address a) possible

admixtures for void elimination and b) the utility of self-compacting concretes for void reduction.

BIBLIOGRAPHY

1. Spellman, D.S. and Stratfull, R.F., "Concrete Variables and Corrosion Testing," *Highway Research Record*, No. 423, 1963, p. 27.

2. Clear, K.C., "Time-to-Corrosion of Reinforcing Steel in Concrete Slabs," Report No. FHWA-RD-76-70, Federal Highway Administration, Washington, D.C., 1976.

3. Hausmann, D.A., *Materials Protection*, Vol. 6(10), 1967, p. 23.

4. Gouda, V.K., *British Corrosion Journal*, Vol. 5, 1970, p. 198.

5. Hausmann, D.A., *Materials Performance*, Vol. 37(10), 1998, p. 64.

6. Breit, W., *Mater. Corrosion*, Vol. 49, 1998, p. 539.

7. Charvin, S., Hartt, W.H., and Lee, S. K., "Influence of Permeability Reducing and Corrosion Inhibiting Admixtures in Concrete upon Initiation of Salt Induced Embedded Steel Corrosion," paper no. 00802 presented at CORROSION/00, March 26-31, 2000, Orlando.

8. Li, L. and Sagüés, A.A., *Corrosion*, Vol. 57, 2001, p. 19.

9. Glass, G.K. and Buenfeld, N.R., "Chloride Threshold Levels for Corrosion Induced Deterioration of Steel in Concrete," paper no. 3 presented at RILEM International Workshop on Chloride Penetration into Concrete, Oct. 15-18, 1995, Saint Rémy-les-Chevreuse.

10. Broomfield, J.P., *Corrosion of Steel in Concrete*, E&FN Spon, London, 1997, pp. 22-25.

11. Tutti, K., *Corrosion of Steel in Concrete*, Report No. Fo 4, Swedish Cement and Concrete Research Institute, Stockholm, 1982.

12. Longuet, P., Burglen, L., and Zelwer, A., *Rev. Matér.*, Vol. 35, 1973, p. 676.

13. Barneyback, R.S. and Diamond, S., *Cem. Concr. Res.*, Vol. 11, 1982, p. 279.

14. Page, C.L. and Vennesland, O., *Mater. Struct.*, Vol. 19, 1983, p. 16.

15. Sagüés, A.A., Moreno, E.I., and Andrade, C., *Cem. Concr. Res.*, Vol. 27, 1997, p. 1747.

16. Li, L., Sagüés, A.A., and Poor, N, *Cem. Concr. Res.*, Vol. 29, 1999, p. 315.

17. Hartt, W.H., Charvin, S., and Lee, S.K., "Influence of Permaeability Reducing and Corrosion Inhibiting Admixtures in Concrete upon Initiation of Salt Induced

Embedded Metal Corrosion," final report submitted to FDOT by FAU on Project WPI 0510716, June 18, 1999.

18. Bamforth, P.B., "Definition of Exposure Classes and Concrete Mix Requirements for Chloride Contaminated Environments," *Corrosion of Reinforcement in Concrete*, Eds: Page, C.L., Treadaway, K.W.J., and Bamforth, P.B., Soc. Chem. Ind., London, 1996, p. 176.

19. Bamforth, P.B. and Price, W.F., "Factors Influencing Chloride Ingress into Marine Structures," *Concrete 2000*, Eds: Dhir, R.K. and Jones, M.R., E&FN Spon, London, 1993, p. 1105.

20. ASTM Standard Test Method G 109-99, "Determining the Effect of Chemical Admixtures on the Corrosion of Embedded Steel Reinforcement in Concrete Exposed to Chloride Environments," Annual Book of ASTM Standards, Vol. 03.02, American Society for Testing and Materials, 100 Barr Harbor Drive, West Conshohocken, PA.

21. "Florida Method of Test for Determining Low-Levels of Chloride in Concrete and Raw Materials," Designation FM 5-516, Florida Department of Transportation, Tallahassee, FL, Sept., 1994.

22. Li, L, Nam, J., and Hartt, W.H., "Ex-Situ Leaching Measurement of Concrete Alkalinity," paper no. 03299 to be presented at CORROSION/03.

23. ASTM Standard Test Method C 642-90, "Test Method for Density, Absorption, and Voids in Hardened Concrete," Annual Book of ASTM Standards, Vol. 04.02, American Society for Testing and Materials, 100 Barr Harbor Drive, West Conshohocken, PA.

24. ASTM Standard Test Method G 876-99, "Test Method for Half-Cell Potentials of Uncoated Reinforcing Steel in Concrete," Annual Book of ASTM Standards, Vol. 03.02, American Society for Testing and Materials, 100 Barr Harbor Drive, West Conshohocken, PA.

25. Hartt, W.H., Nam, J., and Li, L. "A Unified Approach to Concrete Mix Design Optimization for Durability Enhancement and Life-Cycle Cost Optimization," Draft Final Report submitted to FDOT Research Center by Florida Atlantic University, June 13, 2002.

26. Sandberg, P. and Larsson, J., "Chloride Binding in Cement Pastes in Equilibrium with Synthetic Pore Solutions," in, *Chloride Penetration in Concrete Structures*, Ed. L.-O Nilsson, Nordic Miniseminar, Göteborg, 1993, p. 98.

27. Tritthart, J., *Cem. Concr. Res.*, Vol. 19, 1989, p. 683.

28. Diamond, S. *Cem. Concr. Res.*, Vol. 11, 1981, p. 383.

29. Diamond, S., "Effects of Microsilica (Silica Fume) on Pore Solution Chemistry of Cement Pastes," *Communications of Am. Ceramics Soc.*, 1983, p. C82.

30. Arya, C. and Xu, Y. *Cem. Concr. Res.*, Vol. 25, 1995, p. 893.

31. Constantiner, D. and Diamond, S., “Pore Solution Analysis: Are There Pressure Effects,” in *Mechanisms of Chemical Degradation of Cement-based Systems*, Eds: K.L. Scrivener and J.F. Young, E&FN SPON, London, 1997, p. 22.

32. Kawamura, M., Kayyali, O.A., and Haque, M.N., *Cem. Concr. Res.*, Vol. 18, 1988, p. 763.

33. Kayyali, O.A. and Haque, M.N., *J. of Materials in Civil Engr.*, Vol. 2, 1990, p. 24.

34. Larbi, J.A., Fraay, A.L., and Bijen, J.M., *Cem. Concr. Res.*, Vol. 20, 1990, p. 506.

35. Duchesne, J. and Berube, M.A., *Cem. Concr. Res.*, Vol. 24, 1994, p. 456.

36. Bamforth, P., *Corrosion Prevention and Control*, Aug., 1996, p. 91.

37. Monfore, G.E. and Verbeck, G.J., *ACI Journal Proceedings*, Vol. 32, 1960, p. 491.

38. Miller, R.L., Hartt, W.H., and Brown, R.P., *Materials Performance*, Vol. 15(5), 1976, p. 20.